

## Article

# Paleoenvironment of the Lower–Middle Cambrian Evaporite Series in the Tarim Basin and Its Impact on the Organic Matter Enrichment of Shallow Water Source Rocks

Mingyang Wei <sup>1,2</sup>, Zhidong Bao <sup>1,2,\*</sup>, Axel Munnecke <sup>3</sup> , Wei Liu <sup>4</sup>, G. William M. Harrison <sup>5</sup> , Hua Zhang <sup>1,2,6</sup>, Demin Zhang <sup>7</sup>, Zongfeng Li <sup>1,2</sup>, Xiting Xu <sup>1,2</sup>, Kai Lu <sup>1,2</sup> and Zheng Shen <sup>1,2</sup>

- <sup>1</sup> College of Geosciences, China University of Petroleum, Beijing 102249, China; 2016311002@student.cup.edu.cn (M.W.); zhang.hua@mail.cgs.gov.cn (H.Z.); 2018311001@student.cup.edu.cn (Z.L.); 2018211003@student.cup.edu.cn (X.X.); 2017311001@student.cup.edu.cn (K.L.); 2020210002@student.cup.edu.cn (Z.S.)
  - <sup>2</sup> State Key Laboratory of Petroleum Resources and Prospecting, China University of Petroleum, Beijing 102249, China
  - <sup>3</sup> GeoZentrum Nordbayern, Friedrich-Alexander University Erlangen-Nuremberg (FAU), Fachgruppe Palaeoumwelt, Loewenichstr. 28, D-91054 Erlangen, Germany; axel.munnecke@fau.de
  - <sup>4</sup> PetroChina Research Institute of Petroleum Exploration and Development, Beijing 100083, China; liuwei086@petrochina.com.cn
  - <sup>5</sup> Marine Biodiversity, Naturalis Biodiversity Center, 2333 CR Leiden, The Netherlands; william.harrison@naturalis.nl
  - <sup>6</sup> Chinese Academy of Geological Sciences, Beijing 100037, China
  - <sup>7</sup> Sinopec Petroleum Exploration and Production Research Institute, Beijing 100728, China; zhangdm.syky@sinopec.com
- \* Correspondence: baozhd@cup.edu.cn



**Citation:** Wei, M.; Bao, Z.; Munnecke, A.; Liu, W.; Harrison, G.W.M.; Zhang, H.; Zhang, D.; Li, Z.; Xu, X.; Lu, K.; et al. Paleoenvironment of the Lower–Middle Cambrian Evaporite Series in the Tarim Basin and Its Impact on the Organic Matter Enrichment of Shallow Water Source Rocks. *Minerals* **2021**, *11*, 659. <https://doi.org/10.3390/min11070659>

Academic Editors:  
Marcello Natalicchio and Francesco Dela Pierre

Received: 29 April 2021  
Accepted: 14 June 2021  
Published: 22 June 2021

**Publisher's Note:** MDPI stays neutral with regard to jurisdictional claims in published maps and institutional affiliations.



**Copyright:** © 2021 by the authors. Licensee MDPI, Basel, Switzerland. This article is an open access article distributed under the terms and conditions of the Creative Commons Attribution (CC BY) license (<https://creativecommons.org/licenses/by/4.0/>).

**Abstract:** Just as in deep-water sedimentary environments, productive source rocks can be developed in an evaporitic platform, where claystones are interbedded with evaporites and carbonates. However, the impact of the paleoenvironment on the organic matter enrichment of shallow water source rocks in an evaporite series has not been well explored. In this study, two wells in the central uplift of the Tarim Basin were systematically sampled and analyzed for a basic geochemical study, including major elements, trace elements, and total organic carbon (TOC), to understand the relationship between TOC and the paleoenvironmental parameters, such as paleosalinity, redox, paleoclimate, paleo-seawater depth, and paleoproductivity. The results show that the Lower–Middle Cambrian mainly developed in a fluctuating salinity, weak anoxic to anoxic, continuous dry and hot, and proper shallow water environment. The interfingering section of evaporites, carbonates, and claystones of the Awatag Fm. have higher paleoproductivity and higher enrichment of organic matter. Paleosalinity, redox, paleoclimate, paleo-seawater depth, and paleoproductivity jointly control the organic matter enrichment of shallow water source rocks in the evaporite series. The degree of enrichment of organic matter in shallow water source rocks first increases and then decreases with the increase in paleosalinity. All the samples with high content of organic matter come from the shallower environment of the Awatag Fm.

**Keywords:** evaporite series; paleoenvironment; shallow water source rock; Lower–Middle Cambrian; Tarim Basin

## 1. Introduction

People's understanding of the relationship between evaporites and hydrocarbons can be traced back to biblical times when people began to discover and use asphalt near the Dead Sea [1]. The scientific research related to it began in the middle of the last century [2,3]. Later, studies showed that about half of the world's oil and gas fields developed in evaporite series [4–7]. Due to this, people began to pay attention to the influence of evaporative

environments on the hydrocarbon generation potential of source rocks. Based on the study of hypersaline sea-marginal pools in the Red Sea, Friedman et al. believe that the organic matter contained in evaporite provides important source material for hydrocarbons [8]. Svetlana et al. discussed the organic inclusions in the Cambrian evaporite deposit from the southern part of the Siberian platform, and they found four types of hydrocarbon inclusions from the evaporite series [9]. In recent years, some scholars have focused on the lacustrine evaporite series of the Lower Cretaceous in the south Atlantic Ocean [10] and the salinized lacustrine basins in China [11]. They think the evaporitic environment may be beneficial to the formation of saline lacustrine source rocks. However, studies on the impact of the paleoenvironment on the organic matter enrichment of shallow water source rocks in marine evaporite series are still lacking [12–17].

The Lower–Middle Cambrian layers in the platform area of the Tarim Basin are a typical evaporite series in China, with dominant sedimentary facies like ramp, open platform, restricted platform, and evaporitic platform [18–20]. Previous studies on the source rocks of the Cambrian in the Tarim Basin were mainly focused on the black claystones of Lower Cambrian Yuertus Fm., which were developed in ramps and deep-water basins, with TOC between 2% and 6%, and even up to 17% in specific areas [21–24]. As the exploration of Cambrian hydrocarbon accumulations in the Tarim Basin progresses, it became apparent that the Yuertus Fm. which was deposited in relatively deep water, was not the only Cambrian source rock with high hydrocarbon potential in the Tarim Basin.

In this study, the evaporite series of the Lower–Middle Cambrian in wells H4 and ZS1 were systematically sampled. TOC values were assayed in all the samples from both wells. After that, pyrolysis analysis on the samples from well H4 and major/trace elements analysis on the samples from well ZS1, respectively, were conducted. The paleosalinity, redox condition, paleoproductivity, paleoclimate, paleo-seawater depth, and their correlations with organic matter enrichment were analyzed. The main focus is the evaluation of the factors controlling the formation of the shallow water source rocks. This study not only advances the theory of the formation mechanism of shallow water source rocks but also provides guidance for predicting favorable hydrocarbon areas of the Lower–Middle Cambrian evaporite series in the Tarim Basin and evaporitic platform source rocks all over the world.

## 2. Geological Setting

The Tarim Basin is located in northwest China, surrounded by the Tianshan Mountains in the north, the Kunlun Mountains in the south, the Altun Mountains in the east, and the Pamir Plateau in the west (Figure 1a). With an area of  $56 \times 10^4$  km<sup>2</sup>, the basin is the largest sedimentary basin in China [18,25]. Controlled by the breakup of the Rodinia supercontinent, the rifting activities around the Tarim Basin turned the original rift basin gradually into an ocean basin after the “snowball event” in the Neoproterozoic, while the Tarim Basin itself gradually evolved into an intra-cratonic depression basin [26–28]. The palaeogeographic position of the Tarim plate in the Early Cambrian is thought to be in the subtropics of the northern hemisphere [29]. During the early stages of the Early Cambrian, the Tarim Basin gradually changed from a carbonate ramp to a carbonate platform. It turned into an evaporitic platform during the late stages of the Early Cambrian and the Middle Cambrian. The platform area is positioned in today’s western part of the Tarim desert and the basin area in the eastern region of Tarim [21]. There are three large-scale paleouplifts and four paleodepressions separated by them in the Tarim Basin (Figure 1a). They are the north Tarim uplift, central uplift, southeast uplift, Kuka depression, north depression (include Awati Depression and Manjiaer Depression), southwest depression (including Tangguzibasi Depression, etc.), and southeast depression. The central uplift can be subdivided into the Bachu Uplift, the Central Tarim Uplift, and the East Tarim Uplift. The well H4 and well ZS1 studied in this paper are located in the Bachu Uplift and the Central Tarim Uplift, respectively.

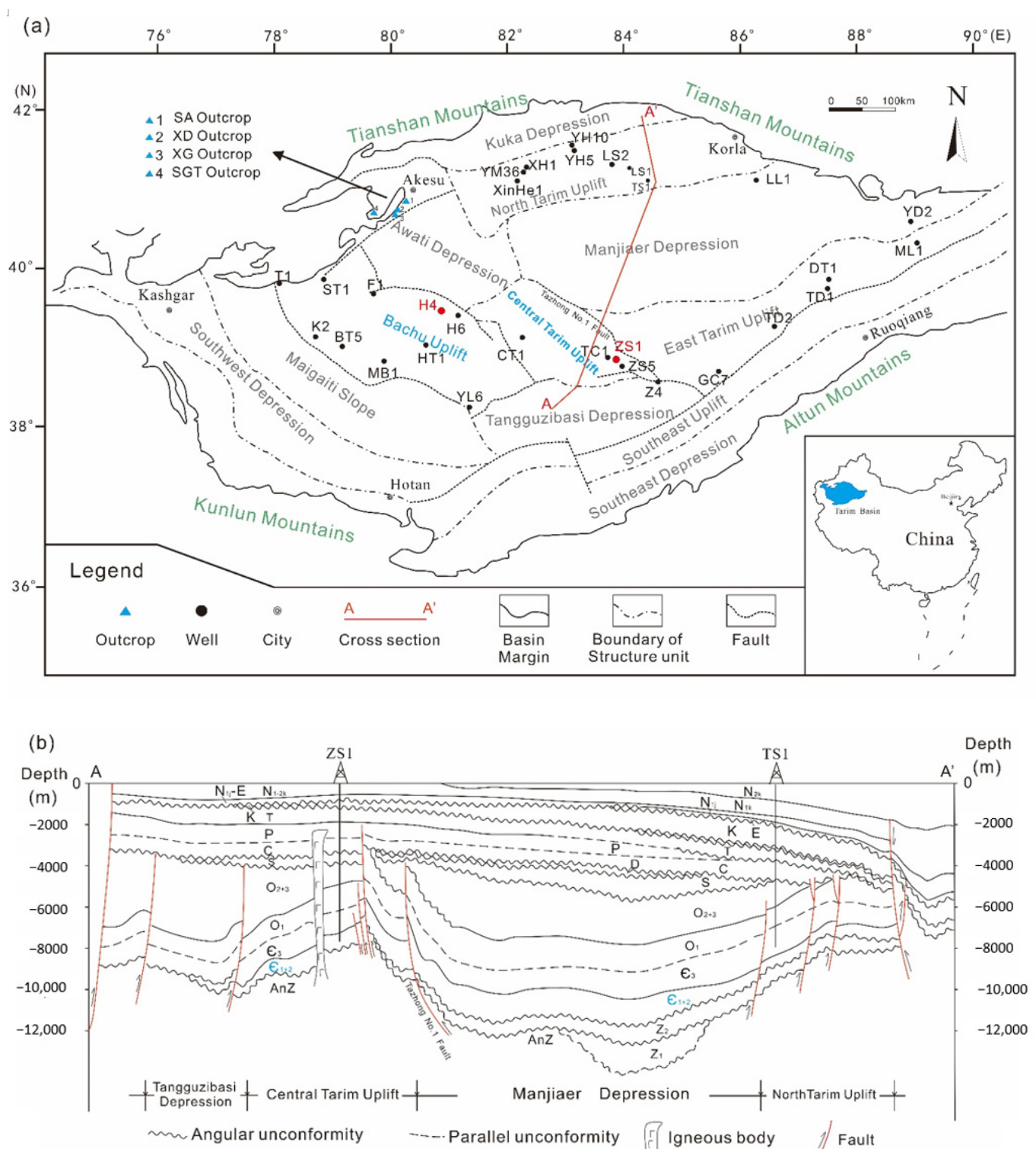


**Figure 1.** Schematic map showing the distribution of the structure units and drilling cores of the Tarim Basin (in stratigraphic symbols, AnZ stands for pre-Sinian, Z for Sinian, E<sub>1+2</sub> for Lower–Middle Cambrian, and E<sub>3</sub> for Upper Cambrian, and other symbols for the strata above Cambrian). (a) The distribution of the structure units, drilling cores, and outcrops [25,26]; (b) north-south stratigraphic section of the Tarim Basin [18,28].

The Cambrian in the Tarim Basin is subdivided into the Lower, Middle, and Upper Cambrian (Figures 2 and 3). The Upper Cambrian corresponds to the upper part of the Maolingian and Furongian, the Middle Cambrian to the lower part of the Maolingian, and the Lower Cambrian to Series 2 and the Terreneuvain. The Lower Cambrian deposits in the

Tarim Basin can be subdivided into the Yuertus ( $C_{1y}$ ), Xiaoerbrak ( $C_{1x}$ ), and Wusongger ( $C_{1w}$ ) Formations (Figure 2) [30,31]. The Yuertus Fm. disconformably overlies Sinian strata (Ediacaran) (Figure 1b), with a relatively small thickness. For example, in the Akesu area, the thickness of the Yuertus Fm. is only about 10 to 20 m. The lower part is mainly composed of silty or siliceous claystones. The middle part consists of phosphorites with thin layers of micritic dolomites. The upper part is composed of black carbonaceous shales, and thin interbeds of shales and argillaceous dolomites [21,32]. The thickness of the overlying Xiaoerbrak Fm. is about 70–140 m. The lower part mainly consists of argillaceous dolomites and micritic dolomites, whereas the upper part is mainly made of fine crystalline dolomites and stromatolitic dolomites. The top part is composed of crystalline dolomites with abundant dissolution pores [33,34]. The thickness of the youngest Lower Cambrian formation, the Wusongger Fm., is similar to that of the Xiaoerbrak Fm., at about 80–145 m. Drilling cores indicate that a large part of the Wusongger Fm. in the inner part of the platform consists of anhydrite and halite, while coeval outcrops in the Akesu area show red claystones deposited at the outer platform [33,35]. The Middle Cambrian in the Tarim Basin is subdivided into the Shayilik ( $C_{2s}$ ) and Awatag ( $C_{2a}$ ) formations. The Shayilik Fm. is a relatively thin limestone unit with a thickness of about 50–100 m. A large number of chert nodules, ranging from 5 to 30 cm in diameter, are observed in the limestones in the outcrop area near Akesu city. Above it, the Awatag Fm. is characterized by very thick evaporite layers of about 150–400 m in thickness [33,36]. The anhydrite and halite layers in this formation are much thicker than those in the Wusongger Fm. However, near Akesu city, there are also non-evaporitic deposit outcroppings such as red claystones interbedding with micritic dolomites and stromatolitic dolomites.

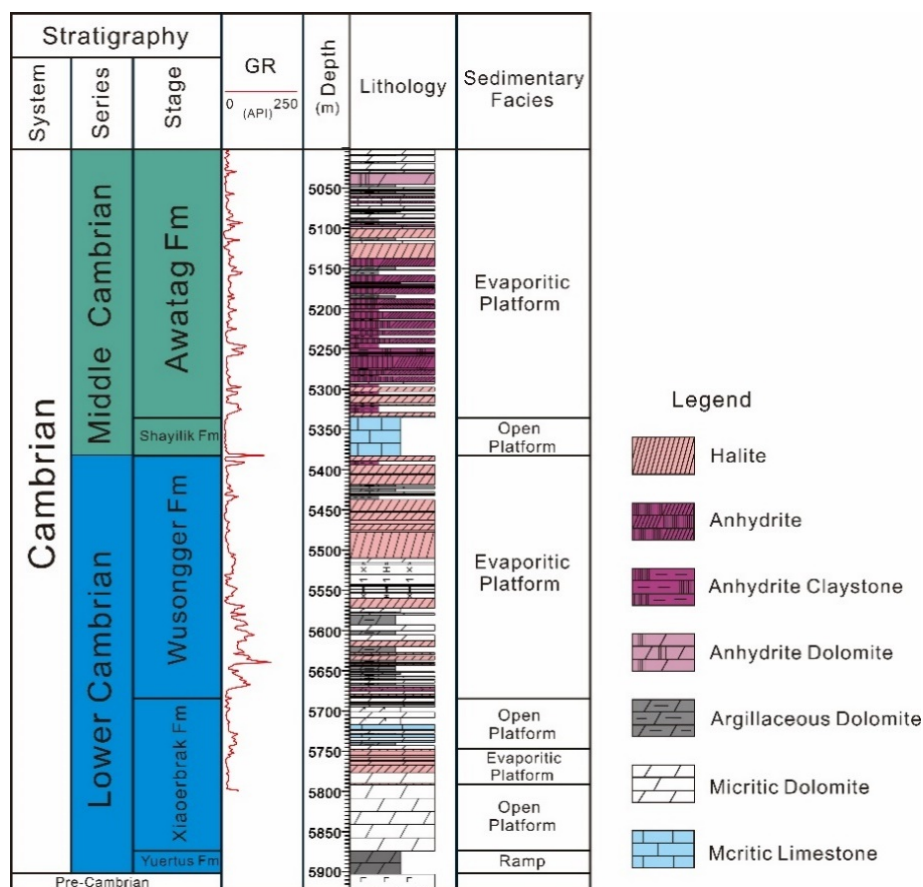
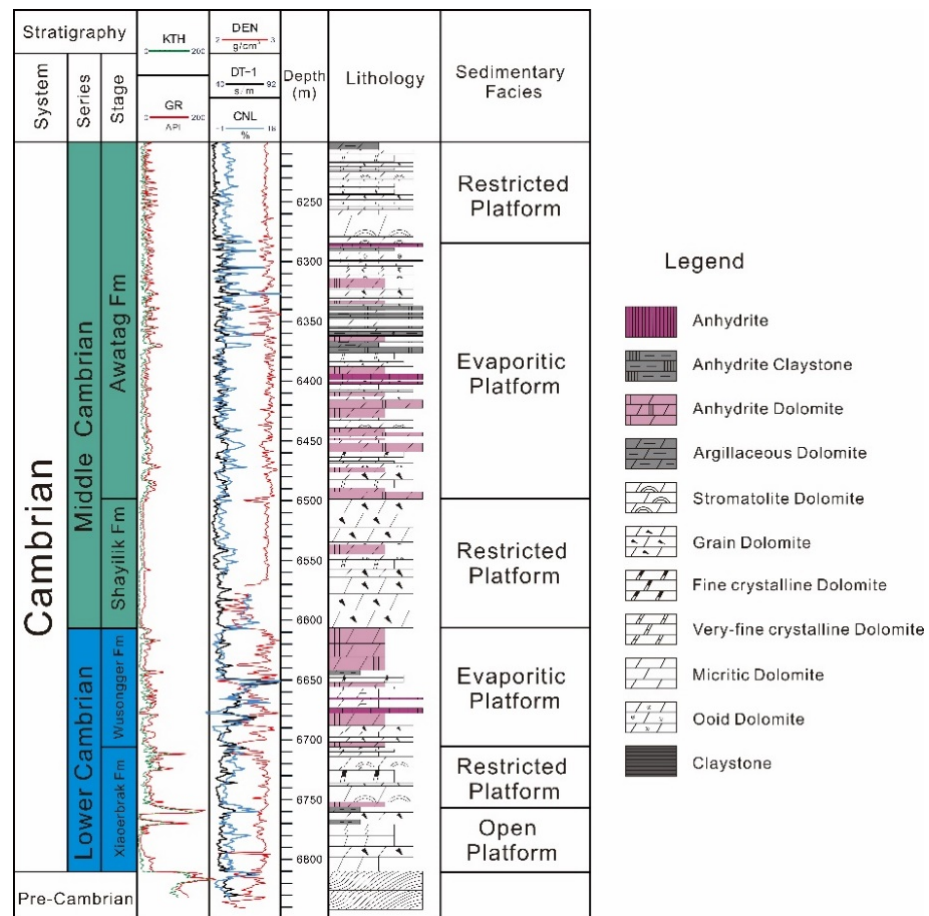


Figure 2. Stratigraphy and lithology of the Lower–Middle Cambrian deposits of well H4 in the Tarim Basin.



**Figure 3.** Stratigraphy and lithology of the Lower–Middle Cambrian deposits of well ZS1 in the Tarim Basin.

Seven sedimentary facies can be distinguished in the Lower–Middle Cambrian evaporite series of the Tarim Basin, which are ramp, platform margin, open platform, restricted platform, evaporitic platform, slope, and basin. Vertically, ramp deposits are mainly distributed in the Yuertus Fm. in the central and western Tarim Basin. In eastern Tarim, the ramp continued throughout the Cambrian period. It can be further subdivided into inner, middle, and outer ramp according to the lithology of sediments. Only very thin layers of claystones or claystones interbedded with limestones or dolomites with a thickness of no more than 10 m were found in the northwestern outcrops and the north Tarim uplift. The platform margin started to take shape during the sedimentary period of Xiaoerbrak Fm., which consists of microbial reefs and shoals. Platform margin deposits are developed from the Xiaoerbrak Fm. to the Awatag Fm. in the north Tarim uplift, east Tarim uplift, and northwestern outcrop area. The formation of the platform margin led to the evolution of the original ramp into a platform. At that time, no pronounced shoals and microbial reefs were developed at the platform margin that affected the water circulation between the platform and the ocean, so it was an open platform. An open platform also formed in the lower part of the Xiaoerbrak Fm. (Figures 2 and 3), and the sediments form most of the Shayilik Fm. Due to the development of shoals and microbial reefs at the platform margin, the originally open platform gradually turned into a semi-closed restricted platform. Restricted platform deposits developed in the Xiaoerbrak Fm., usually represented by abundant intra-platform shoals. During the deposition of the Wusongger Formation, the platform margin gradually separated the platform from the ocean. Surrounded and restricted by the platform margin and the subaerially exposed area, a relatively closed sedimentary environment formed in the central platform area. Due to a dry and hot climate, the salinity increased continuously

until gypsum and halite precipitated in some sort of very large inner platform salina. Together with dolomite flats, they eventually formed a large evaporitic platform (Figure 4). Evaporitic platforms are common in the Wusongger Fm. and the Awatag Fm., representing the precipitates from inner platform salina pans. Such salina areas have been discovered in the area near well H4. The deep-water basin was located in the Manjiaer Depression and Kuka Depression.

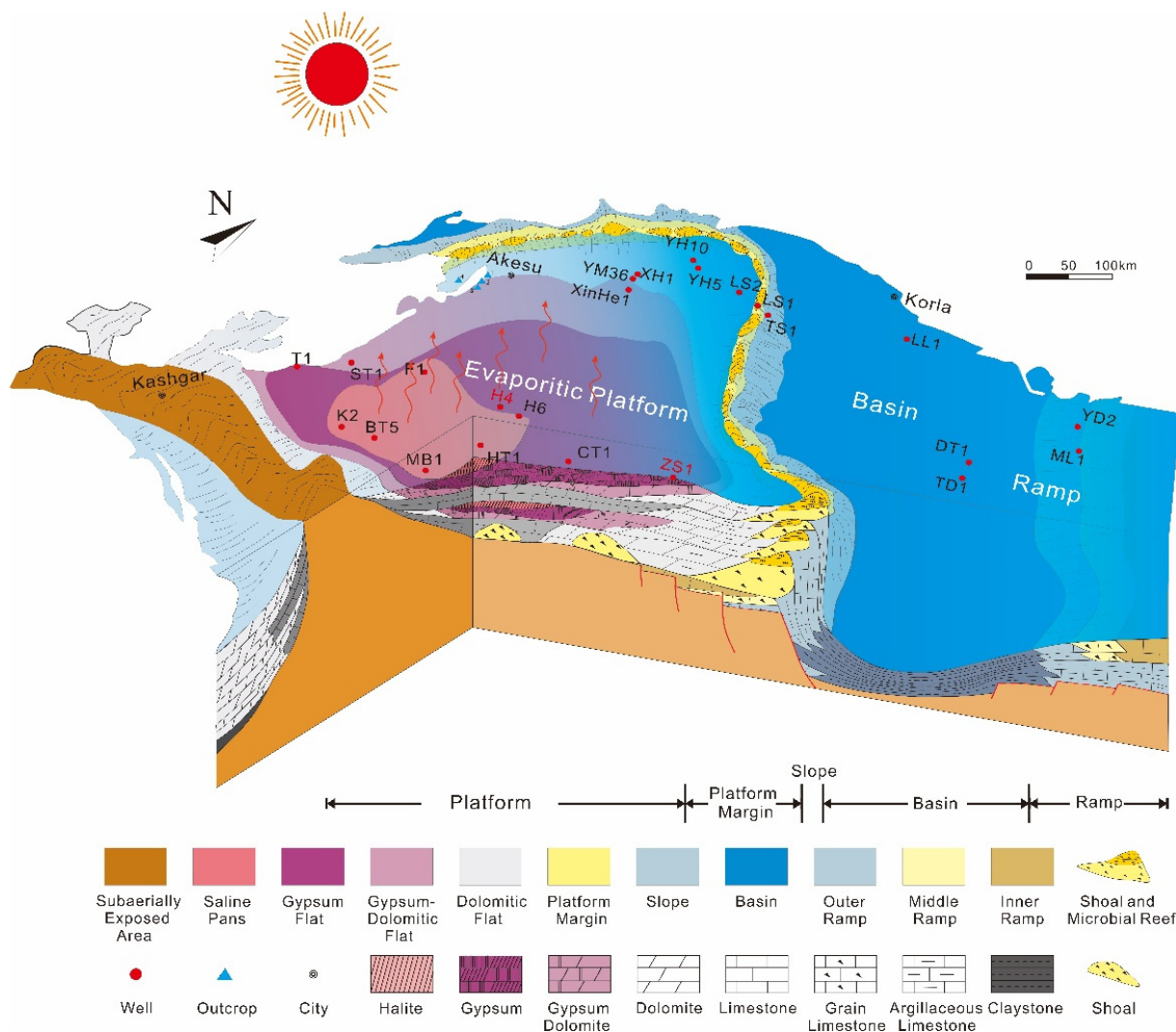


Figure 4. A 3-D sedimentary model of the evaporite-carbonate platform of Early Middle Cambrian in the Tarim Basin.

### 3. Materials and Methods

#### 3.1. Samples

Two hundred and twenty-one samples were collected from the XD, SA, XG, and SGT outcrops near Akesu city, which is located in the northwest of the Tarim Basin (Figure 1). About 550 m of drilling cores of wells CT1, ZS1, and ZS5 in the Central Tarim Uplift, wells K2, F1, H4, H6, and ST1 in the Bachu Uplift, and wells XH1, Xinhe1, YH5, and YH10 in the North Tarim Uplift have been observed and described, and 154 core samples were collected. From well H4 (Figures 1 and 2), 54 core samples were collected for TOC and pyrolysis (Table 1). From well ZS1 (Figures 1 and 3), 56 core samples were collected for TOC, major element, and trace element analysis (Table 2). All the samples were pulverized to <200 mesh sizes.

**Table 1.** Location, lithology, and basic geochemical data for the 54 core samples From Lower–Middle Cambrian of well H4, Tarim Basin.

No.	Depth (m)	Formation	Lithology	TOC (%)	T <sub>max</sub> (°C)	S <sub>1</sub> (mg/g)	S <sub>2</sub> (mg/g)	S <sub>1</sub> + S <sub>2</sub> (mg/g)	S <sub>3</sub> (mg/g)	HI (mg/g TOC)	OI (mg/g TOC)
1	5025	E <sub>2a</sub>	micritic dolomite	0.35	428	0.09	0.24	0.33	0.68	69	194
2	5035	E <sub>2a</sub>	micritic dolomite	0.4	415	0.06	0.2	0.26	1.1	50	275
3	5045	E <sub>2a</sub>	micritic dolomite	0.22	426	0.09	0.17	0.26	0.68	77	309
4	5055	E <sub>2a</sub>	micritic dolomite	0.18	420	0.1	0.15	0.25	0.55	83	306
5	5065	E <sub>2a</sub>	anhydrite dolomite	0.58	443	0.21	1.02	1.23	0.83	176	143
6	5075	E <sub>2a</sub>	anhydrite dolomite	0.5	440	0.37	0.83	1.2	0.84	166	168
7	5085	E <sub>2a</sub>	micritic dolomite	0.35	429	0.08	0.28	0.36	1.03	80	294
8	5095	E <sub>2a</sub>	micritic dolomite	0.22	445	0.28	0.5	0.78	0.44	227	200
9	5105	E <sub>2a</sub>	micritic dolomite	0.31	422	0.15	0.25	0.4	0.57	81	184
10	5115	E <sub>2a</sub>	micritic dolomite	0.47	428	0.77	0.78	1.55	0.66	166	140
11	5135	E <sub>2a</sub>	micritic dolomite	0.42	416	0.15	0.4	0.55	0.9	95	214
12	5145	E <sub>2a</sub>	anhydrite claystone	1.44	406	0.22	2.21	2.43	5.73	153	398
13	5155	E <sub>2a</sub>	anhydrite claystone	1.31	403	0.2	1.79	1.99	5.98	137	456
14	5165	E <sub>2a</sub>	anhydrite claystone	1.44	425	0.14	1.77	1.91	5.03	123	349
15	5175	E <sub>2a</sub>	anhydrite dolomite	0.24	427	0.04	0.11	0.15	0.73	46	304
16	5185	E <sub>2a</sub>	anhydrite dolomite	0.35	420	0.07	0.26	0.33	1.15	74	329
17	5195	E <sub>2a</sub>	anhydrite dolomite	0.47	430	0.08	0.44	0.52	1.54	94	328
18	5205	E <sub>2a</sub>	micritic dolomite	0.37	405	0.07	0.34	0.41	1.34	92	362
19	5215	E <sub>2a</sub>	argillaceous dolomite	1.74	413	0.63	2.49	3.12	3.88	143	223
20	5225	E <sub>2a</sub>	anhydrite dolomite	1.18	406	0.48	1.67	2.15	2.57	142	218
21	5235	E <sub>2a</sub>	anhydrite claystone	7	/	39.3	66.04	105.34	63.91	199	192
22	5245	E <sub>2a</sub>	anhydrite dolomite	0.31	432	0.07	0.25	0.32	1.17	81	377
23	5255	E <sub>2a</sub>	anhydrite dolomite	0.53	416	0.1	0.29	0.39	1.53	55	289
24	5265	E <sub>2a</sub>	anhydrite dolomite	0.61	438	0.2	0.47	0.67	0.91	77	149
25	5275	E <sub>2a</sub>	anhydrite dolomite	1.04	438	0.36	1.4	1.76	2	135	192
26	5285	E <sub>2a</sub>	anhydrite dolomite	0.48	432	0.08	0.42	0.5	2.52	88	525
27	5295	E <sub>2a</sub>	micritic dolomite	0.23	425	0.04	0.14	0.18	0.72	61	313
28	5345	E <sub>2s</sub>	micritic limestone	0.98	425	0.23	0.62	0.85	2.85	63	291
29	5355	E <sub>2s</sub>	micritic limestone	0.41	431	0.07	0.23	0.3	2.01	56	490
30	5375	E <sub>2s</sub>	micritic limestone	0.22	412	0.14	0.14	0.28	0.55	64	250
31	5525	E <sub>1w</sub>	micritic dolomite	0.2	607	0.02	0.05	0.07	0.56	25	280
32	5555	E <sub>1w</sub>	micritic dolomite	0.08	516	0.03	0.06	0.09	0.91	75	1138
33	5575	E <sub>1w</sub>	anhydrite dolomite	0.25	399	0.02	0.08	0.1	0.46	32	184
34	5585	E <sub>1w</sub>	micritic dolomite	0.72	400	0.05	0.06	0.11	0.5	8	69
35	5595	E <sub>1w</sub>	micritic dolomite	0.91	396	0.03	0.07	0.1	0.64	8	70

Table 1. Cont.

No.	Depth (m)	Formation	Lithology	TOC (%)	T <sub>max</sub> (°C)	S <sub>1</sub> (mg/g)	S <sub>2</sub> (mg/g)	S <sub>1</sub> + S <sub>2</sub> (mg/g)	S <sub>3</sub> (mg/g)	HI (mg/g TOC)	OI (mg/g TOC)
36	5605	E <sub>1w</sub>	micritic dolomite	0.58	405	0.03	0.06	0.09	0.62	10	107
37	5615	E <sub>1w</sub>	micritic dolomite	0.76	/	0.02	0.08	0.1	1	11	132
38	5625	E <sub>1w</sub>	micritic dolomite	0.79	394	0.06	0.15	0.21	0.79	19	100
39	5635	E <sub>1w</sub>	micritic dolomite	0.9	408	0.23	0.53	0.76	1.68	59	187
40	5645	E <sub>1w</sub>	micritic dolomite	0.74	607	0.05	0.05	0.1	0.48	7	65
41	5655	E <sub>1w</sub>	micritic dolomite	0.27	606	0.01	0.06	0.07	0.65	22	241
42	5665	E <sub>1w</sub>	micritic dolomite	0.58	606	0.02	0.09	0.11	1.11	16	191
43	5675	E <sub>1w</sub>	argillaceous dolomite	2.32	422	1.83	2.51	4.34	4.13	108	178
44	5685	E <sub>1x</sub>	micritic dolomite	1.18	415	0.5	1.27	1.77	2.76	108	234
45	5695	E <sub>1x</sub>	micritic dolomite	0.41	411	0.04	0.16	0.2	1.07	39	261
46	5705	E <sub>1x</sub>	micritic dolomite	0.3	415	0.04	0.13	0.17	0.71	43	237
47	5715	E <sub>1x</sub>	micritic dolomite	0.28	416	0.03	0.13	0.15	0.92	46	329
48	5725	E <sub>1x</sub>	micritic dolomite	0.24	416	0.03	0.12	0.15	0.69	50	288
49	5735	E <sub>1x</sub>	micritic dolomite	0.34	400	0.02	0.1	0.12	0.63	29	185
50	5745	E <sub>1x</sub>	micritic dolomite	0.34	413	0.09	0.19	0.28	0.65	56	191
51	5755	E <sub>1x</sub>	micritic dolomite	0.71	410	0.11	0.33	0.44	0.95	46	134
52	5765	E <sub>1x</sub>	micritic dolomite	0.55	396	0.2	0.43	0.63	1.36	78	247
53	5785	E <sub>1x</sub>	anhydrite dolomite	0.78	406	0.31	0.59	0.9	1.03	76	132
54	5795	E <sub>1x</sub>	micritic dolomite	0.52	412	0.13	0.48	0.61	1.24	92	238

Table 2. Location, lithology, TOC, major element, and trace element data for the 56 shallow water core samples from Lower–Middle Cambrian of well ZS1, Tarim Basin.

No.	Depth (m)	Formation	Lithology	TOC (%)	Al <sub>2</sub> O <sub>3</sub> (%)	MgO (%)	CaO (%)	V (ppm)	Cr (ppm)	Mn (ppm)	Ni (ppm)	Cu (ppm)	Zn (ppm)	Sr (ppm)	Ba (ppm)	Th (ppm)	U (ppm)	CaO/(Al <sub>2</sub> O <sub>3</sub> +MgO)	V/(V+Ni)	Cu/Zn	Sr/Ba	Sr/Cu	Th/U
1	6217	E <sub>2a</sub>	argillaceous dolomite	0.35	0.06	21.03	28.43	5.8	7.1	41.46	4.37	1.55	43.1	85.5	195	0.43	0.86	1.35	0.57	0.04	0.44	55	0.50
2	6227	E <sub>2a</sub>	stromatolite dolomite	1.12	0.15	18.74	25.77	7.97	10.27	55.32	5.14	6.11	403	91.6	641	0.58	0.96	1.36	0.61	0.02	0.14	15	0.61
3	6237	E <sub>2a</sub>	very-fine crystalline dolomite	0.8	0.02	15.11	33.9	5.57	7.66	47.96	4.61	1.26	108	191	0.41	0.8	2.24	0.55		0.57	86	0.51	
4	6247	E <sub>2a</sub>	grain dolomite	0.11	0.25	19.59	29.55	6.64	7.24	57.02	4.99	2.79	9.24	93.8	206	0.49	0.89	1.49	0.57	0.30	0.45	34	0.55
5	6257	E <sub>2a</sub>	micritic dolomite	0.17	1.43	18.48	25.48	16	16.01	144.01	7.16	5.43	32.5	990	863	1.83	1.41	1.28	0.69	0.17	1.15	182	1.30
6	6267	E <sub>2a</sub>	stromatolite dolomite	0.4	0.31	20.74	28.35	6.77	6.94	65.18	4.65	4.1	148	496	0.56	1.14	1.35	0.59		0.30	36	0.49	
7	6277	E <sub>2a</sub>	stromatolite dolomite	0.11	0.37	20.01	27.15	6.33	6.64	61.28	4.26	3.19	8.61	2947	954	0.54	1.2	1.33	0.60	0.37	3.09	925	0.45
8	6287	E <sub>2a</sub>	gypsum	0.7	0.37	19.39	26.21	9.93	11.35	67.46	6.72	4.45	39.7	956	2315	0.63	1.64	1.33	0.60	0.11	0.41	215	0.39
9	6297	E <sub>2a</sub>	Ooid dolomite	2.78	0.84	18.79	25.16	11.2	13.4	73.83	6.27	4.13	5.81	793	674	0.79	1.79	1.28	0.64	0.71	1.18	192	0.44
10	6307	E <sub>2a</sub>	grain dolomite	0.26	0.16	19.37	26.58	8.26	23.33	91.04	8.8	3.6	71.4	1885	639	0.52	1.77	1.36	0.48	0.05	2.95	524	0.29
11	6317	E <sub>2a</sub>	gypsum dolomite	0.26	0.23	20.63	27.99	6.35	9.59	64.10	5.41	3.35	17.5	2535	338	0.51	1.48	1.34	0.54	0.19	7.49	758	0.34
12	6327	E <sub>2a</sub>	grain dolomite	7.06	0.34	16	21.09	9.97	10.98	59.06	5.36	3.27	14.1	3376	660	0.78	1.54	1.29	0.65	0.23	5.11	1032	0.50
13	6337	E <sub>2a</sub>	grain dolomite	0.29	1.18	19.32	26.51	11.3	10.58	78.63	5.67	3.31	5.52	8618	1162	1.28	1.61	1.29	0.67	0.60	7.41	2600	0.80
14	6347	E <sub>2a</sub>	gypsum claystone	0.13	0.2	19.77	27.34	4.61	5.41	54.81	4.01	1.29	40.0	2606	282	0.41	1.56	1.37	0.54	0.03	9.24	2023	0.26
15	6357	E <sub>2a</sub>	argillaceous dolomite	0.17	0.37	19.69	27.16	5.67	5.66	60.42	4.31	3.09	27.4	3284	507	0.52	1.33	1.35	0.57	0.11	6.47	1063	0.39
16	6367	E <sub>2a</sub>	gypsum dolomite	3.1	1.5	17.45	20.58	18.8	21.04	93.97	8.55	6.06	26.1	3358	699	2.2	1.76	1.09	0.69	0.23	4.80	554	1.25

Table 2. Cont.

No.	Depth (m)	Formation	Lithology	TOC (%)	Al <sub>2</sub> O <sub>3</sub> (%)	MgO (%)	CaO (%)	V (ppm)	Cr (ppm)	Mn (ppm)	Ni (ppm)	Cu (ppm)	Zn (ppm)	Sr (ppm)	Ba (ppm)	Th (ppm)	U (ppm)	CaO/(Al <sub>2</sub> O <sub>3</sub> +MgO)	V/(V+Ni)	Cu/Zn	Sr/Ba	Sr/Cu	Th/U
17	6377	E <sub>2a</sub>	very-fine crystalline dolomite	0.25	0.38	20	27.95	7.12	7.46	57.41	4.95	3.87	10.5	2044	1326	0.66	2.71	1.37	0.59	0.37	1.54	528	0.24
18	6387	E <sub>2a</sub>	grain dolomite	0.37		20.49	28.28	4.92	6.6	55.88	5.21	1.51	90.3	1501	320	0.43	2.18	1.38	0.49	0.02	4.69	995	0.20
19	6397	E <sub>2a</sub>	gypsum	0.12		19.98	28.1	4.81	4.79	49.73	4.32	3.86	53	1931	364	0.35	1.99	1.41	0.53	0.07	5.30	500	0.18
20	6407	E <sub>2a</sub>	micritic dolomite	1.83	0.39	18.31	25.7	8.89	8.48	60.67	5.48	4.38	30.8	728	812	0.64	1.85	1.37	0.62	0.14	0.90	166	0.35
21	6417	E <sub>2a</sub>	gypsum dolomite	0.62	0.07	19.12	27.42	6.07	6.28	44.96	4.72	2.44	-1.32	2350	438	0.68	1.35	1.43	0.56		5.37	962	0.50
22	6427	E <sub>2a</sub>	gypsum dolomite	1.7		21.42	28.15	3.29	6.2	38.25	4.44	1.05	45.1	3586	347	0.2	1.4	1.31	0.43	0.02	10.32	3405	0.15
23	6437	E <sub>2a</sub>	stromatolite dolomite	0.27		20.66	29.05	3.05	4.93	37.49	3.12	2.76	57.6	1261	3465	0.22	1.25	1.41	0.49	0.05	0.36	457	0.18
24	6447	E <sub>2a</sub>	argillaceous dolomite	0.38	0.3	17.68	27.40	7.88	7.19	61.46	4.9	1.57	1.28	2779	372	0.89	1.44	1.52	0.62	1.22	7.46	1774	0.62
25	6457	E <sub>2a</sub>	gypsum dolomite	0.40	0.38	20.41	28.04	8.95	16.44	70.27	4.84	1.85		3093	410	0.74	2.03	1.35	0.65		7.54	1669	0.37
26	6467	E <sub>2a</sub>	micritic dolomite	0.15	0.02	22.38	29.92	3.26	4.84	41.24	3.81	1.29		95.3	234	0.16	0.45	1.34	0.46		0.41	74	0.35
27	6477	E <sub>2a</sub>	grain dolomite	0.24	0.15	19.98	29.18	5.86	11.21	63.90	4.42	6.95		422	3594	0.39	1.66	1.45	0.57		0.12	61	0.24
28	6487	E <sub>2a</sub>	very-fine crystalline dolomite	0.2	1.95	15.59	25.36	16.7	16.09	100.06	7.77	5.34	91.9	3565	1634	2	1.75	1.45	0.68	0.06	2.18	668	1.14
29	6497	E <sub>2a</sub>	gypsum dolomite	0.4	0.06	21.38	28.72	4.71	5.36	55.33	3.9	1.19		107	353	0.3	1.07	1.34	0.55		0.30	90	0.28
30	6507	E <sub>2s</sub>	grain dolomite	0.23	0	22.06	29.74	3.58	7.87	45.08	3.61	4.14	14.3	132	1728	0.17	0.48	1.35	0.50	0.29	0.08	32	0.36
31	6527	E <sub>2s</sub>	grain dolomite	0.1	0.03	22.07	29.75	4.23	6.74	42.30	3.66	1.55	20.1	123	502	0.16	0.48	1.35	0.54	0.08	0.25	80	0.34
32	6537	E <sub>2s</sub>	gypsum dolomite	0.23	0.03	22.08	29.7	5.34	26.28	54.75	4.85	4.1		139	2720	0.29	0.58	1.34	0.52		0.05	34	0.49
33	6547	E <sub>2s</sub>	stromatolite dolomite	1.85	0.1	21.89	29.77	5.64	15.27	47.35	3.95	5.45	23.1	102	3895	0.19	0.31	1.35	0.59	0.24	0.03	19	0.62
34	6557	E <sub>2s</sub>	very-fine crystalline dolomite	0.98	0.05	21.44	29.23	5.08	7.19	49.07	4.4	58	7.32	52.3	450	0.17	0.5	1.36	0.54	7.93	0.12	1	0.34
35	6567	E <sub>2s</sub>	grain dolomite	0.21	0.11	22.24	29.86	4.47	12.41	40.59	4.82	1.61	15	78.4	1112	0.26	0.64	1.34	0.48	0.11	0.07	49	0.41
36	6577	E <sub>2s</sub>	grain dolomite	0.21	0.07	22.41	29.8	4.25	8.93	35.63	4.41	1.49	8.15	76	219	0.23	0.5	1.33	0.49	0.18	0.35	51	0.45
37	6587	E <sub>2s</sub>	grain dolomite	0.13	0.07	22.44	29.89	4.74	7.88	34.33	4.66	0.79		45.7	159	0.29	0.62	1.33	0.50		0.29	58	0.47
38	6597	E <sub>2s</sub>	grain dolomite	0.14	0.08	22.45	29.66	5.62	7.11	29.45	4.99	1.08	7.08	54.7	202	0.31	0.89	1.32	0.53	0.15	0.27	51	0.34
39	6607	E <sub>2s</sub>	gypsum dolomite	0.3	0.12	22.08	29.47	9.39	24.99	63.56	9.66	11.9	35.1	786	1722	0.58	2.18	1.33	0.49	0.34	0.46	66	0.27
40	6617	E <sub>1w</sub>	gypsum dolomite	0.24	0.45	18.97	27.65	8.55	12.42	50.53	4.45	3.9	9.99	1048	1116	0.37	1.81	1.42	0.66	0.39	0.94	269	0.20
41	6627	E <sub>1w</sub>	gypsum dolomite	0.37	0.18	20.26	28.54	13.1	11.87	75.16	6.14	2.97	7.76	7408	2980	1.53	1.9	1.4	0.68	0.38	2.49	2493	0.81
42	6637	E <sub>1w</sub>	gypsum dolomite	0.2	1.11	11.18	27.37	11.9	23.3	70.87	5.71	7.48	10.9	740	1202	1.06	1.77	2.23	0.68	0.68	0.62	99	0.60
43	6647	E <sub>1w</sub>	fine crystalline dolomite	0	0.73	19.14	27.64										1.39						
44	6657	E <sub>1w</sub>	very-fine crystalline dolomite	0.30	0.35	18.79	25.89	17.2	31.51	69.10	6.1	9.99	13.3	725	1113	1.01	1.78	1.35	0.74	0.75	0.65	73	0.57
45	6667	E <sub>1w</sub>	argillaceous dolomite	0.25	0.8	19.97	27.41	9.09	13.11	49.49	3.92	3.44		875	961	1.09	1.46	1.32	0.70		0.91	254	0.75
46	6687	E <sub>1w</sub>	gypsum dolomite	0.25	1.02	20.16	26.86	16.3	12.21	89.96	6.05	5.85	43.1	2001	3475	1.79	1.73	1.27	0.73	0.14	0.58	342	1.03
47	6697	E <sub>1w</sub>	argillaceous dolomite	0.19	1.21	18.02	26.26	14	10.09	86.74	6.71	5.23	34.5	170	269	2.17	2.29	1.37	0.68	0.15	0.63	32	0.95
48	6707	E <sub>1w</sub>	argillaceous dolomite	0.21	1.59	19.27	24.48	15.9	11.47	84.62	7.33	4.95	16.2	261	848	2.17	2.49	1.17	0.68	0.31	0.31	53	0.87
49	6717	E <sub>1x</sub>	stromatolite dolomite	0.28	5.98	13.31	17.3	43.7	54.08	178.32	25.5	19.1	22	97.2	509	7.01	2.29	0.9	0.63	0.87	0.19	5	3.06
50	6727	E <sub>1x</sub>	very-fine crystalline dolomite	0.17	3.1	18.21	24.34	19.8	16.29	148.72	8.57	4.71	3.34	63.6	157	3.04	1.16	1.14	0.70	1.41	0.40	14	2.62
51	6737	E <sub>1x</sub>	grain dolomite	0.35	2.42	18.52	24.73	20.6	59.09	163.81	9.36	3.98		54.2	208	2.73	1.12	1.18	0.69		0.26	14	2.43
52	6747	E <sub>1x</sub>	stromatolite dolomite	0.2	3.28	17.86	23.72	23.3	22.7	167.44	10.7	5.63		57.1	223	3.67	1.61	1.12	0.68		0.26	10	2.28
53	6777	E <sub>1x</sub>	grain dolomite	0.27	3.15	17.10	22.92	24.7	20.87	197.25	7.89	4.49		599	1039	4.05	1.45	1.13	0.76		0.58	133	2.80
54	6787	E <sub>1x</sub>	grain dolomite	0.33	0.6	20.84	28.27	9.79	10	253.67	5.61	1.69	10.6	75.9	604	1.07	0.67	1.32	0.64	0.16	0.13	45	1.60
55	6797	E <sub>1x</sub>	grain dolomite	0.29	0.04	21.37	28.74	6.16	10.4	273.33	6.02	1.21	22	80.5	355	0.53	0.93	1.34	0.51	0.06	0.23	66	0.57
56	6807	E <sub>1x</sub>	micritic dolomite	0.41	2.68	18.55	25.11	20.3	34.36	272.17	6.82	6.66	25.3	44.5	394	1.47	1.62	1.18	0.75	0.26	0.11	7	0.91

### 3.2. Experimental Methods

#### 3.2.1. TOC

For TOC, the carbonate components were first removed using 15% HCl for over 24h. After that, the samples were taken out and rinsed repeatedly with distilled water until the solvent was neutral. Then, the solid residues were then dried in an oven at 60–80 °C. Lastly, the analysis was conducted with a Leco CS-230 carbon–sulfur analyzer. For pyrolysis, an OGE-II Rock-Eval analyzer was used to measure various parameters, including free hydrocarbons ( $S_1$ ), retained hydrocarbons ( $S_2$ ), generated carbon dioxide ( $S_3$ ), and temperature of maximum pyrolysis yield ( $T_{max}$ ). The  $S_1$  is the content of liquid hydrocarbon expelled from the samples at temperatures up to 300 °C, which includes the bitumen already present in the rock; the  $S_2$  is the content of hydrocarbon decomposed at temperatures from 300 to 600 °C, which is an indicator of the potential of the rock to generate additional oil and gas; the  $S_3$  is the content of carbon dioxide generated during pyrolysis, which is thought to be related to the amount of oxygen in the pyrolyzed organic matter. Additional Rock-Eval parameters included the hydrogen index (HI), defined as the product  $100/(S_2/TOC)$ , and the oxygen index (OI), defined as the product  $100(S_3/TOC)$ .

#### 3.2.2. Major Elements

Major elements, including aluminum trioxide ( $Al_2O_3$ ), magnesium oxide (MgO), and calcium oxide (CaO), were determined by an AXIOS-Minerals XRF spectrometer. During the experiment, the samples were fused at 1150 °C to create a glass disc with an M-4 gas automatic melting machine. The analytical precision for major elements was generally better than 5% utilizing GSR-1, GSR-2, and GSR-3 as standard reference materials.

#### 3.2.3. Trace Elements

Trace element analysis was performed by using an Agilent 7500Ce inductively coupled plasma mass spectrometer (ICP-MS). For this analysis, the samples were dissolved by a mixed acid solution of  $HNO_3$ , HF, and  $HClO_4$ . The relative indeterminacies of these tests were less than 5% utilizing GSR-1, GSR-6, GSR-12, and GSR-13 as standard reference materials. The parameters including vanadium (V), chromium (Cr), manganese (Mn), nickel (Ni), copper (Cu), zinc (Zn), strontium (Sr), barium (Ba), thorium (Th), and uranium (U) were measured.

## 4. Results

### 4.1. Petrology

Most Early Middle Cambrian sediments of the evaporite series in the Tarim Basin are evaporites, carbonates, and claystones. The evaporites are mostly composed of halite (Figure 5a), anhydrite (Figure 5b), and mixed sediments with at least 50% anhydrite (Figure 5c,d). Among them, anhydrite is supposed to be formed by dehydration of gypsum precipitated from seawater, which occurs during a long period of burial diagenesis. The main mineral component of the anhydrite mixture is anhydrite, which is often associated with dolomite (Figure 5c,d) and clay. Evaporites are most widespread in the central Tarim uplift and the Bachu Uplift in the Wusonger Fm. and Awatag Fm. The carbonates include dolomites (Figure 6a–c) and limestones (Figure 6d). Dolomites are the most widely distributed Lower–Middle Cambrian rocks in the Tarim Basin. They occur in various formations in most areas of the basin and can be subdivided into stromatolitic dolomite, grain dolomites (or mimetically dolomitized grainstones), micritic dolomites, crystalline dolomites, and dolomites mixed with gypsum or claystone, in which the proportion of dolomite is more than 50%. Dolomitized ooidal and peloidal grainstones, as well as oncoidal rudstones, are mainly found in the Xiaerbrak Formation. Micritic dolomites and crystalline dolomites are observed in almost every formation. Limestones are mainly developed in the Shayilik Fm. (Figure 6d), with a small thickness but a wide distribution, and exist in the central Tarim uplift, the Bachu Uplift, the northern Tarim Uplift, and

in the outcrop area in the northwest of the Tarim Basin. The claystones (Figure 7) can be subdivided into normal claystones, anhydrite claystones (Figure 7a), and dolomitic claystones. Conceptually, the latter two are both claystones with a clay content of more than 50% and contain dolomite, anhydrite, and other associated minerals. The anhydrite claystones were found in the Wusongger Fm. and the Awatag Fm., whereas the dolomitic claystones were found in almost all the Lower–Middle Cambrian evaporite series.

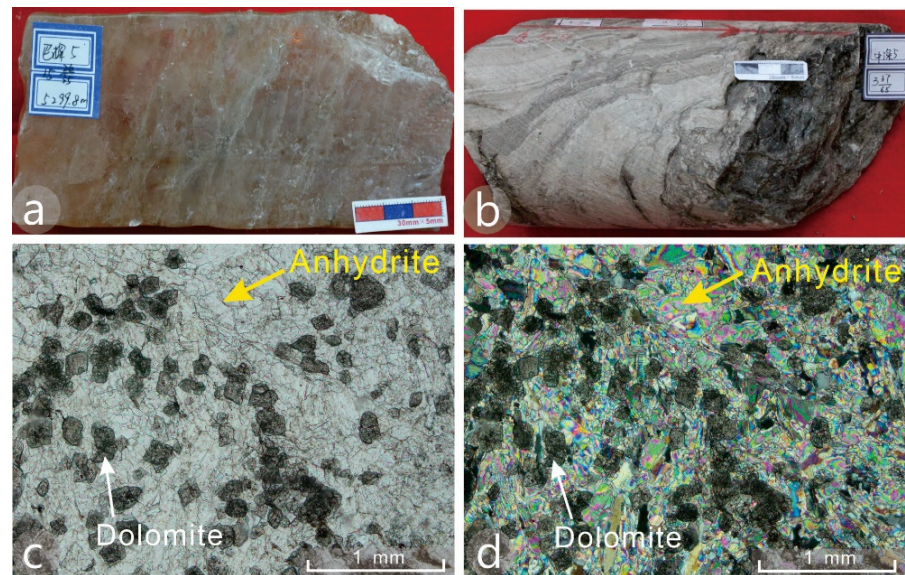


**Figure 5.** Typical evaporites from the Lower–Middle Cambrian in the Tarim Basin. (a) Halite, Awatag Fm., well BT5 (5299.8 m); (b) anhydrite, Awatag Fm., well ZS5 (6193 m); (c) dolomitic gypsum, thin section (transmitted light) Wusongger Fm., well ZS5 (6600 m); (d) same area as in C but with crossed polars.

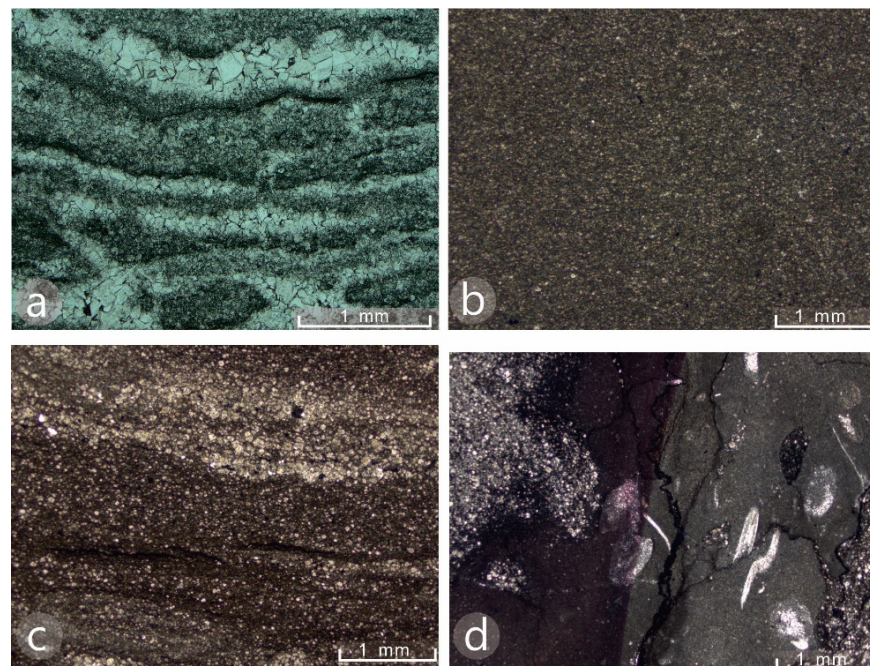


**Figure 6.** Thin sections (transmitted light) of typical Lower–Middle Cambrian carbonates in the Tarim Basin. (a) Stromatolitic dolomite, Xiaerbrak Fm., well ST1 (1885 m); (b) dolomicrite, Xiaerbrak Fm., well XH1 (5789 m); (c) argillaceous dolomite, Wusongger Fm., well YH5 (6022 m); (d) bioclastic dolomitic limestone, Shayilik Fm., well K2 (5291 m).

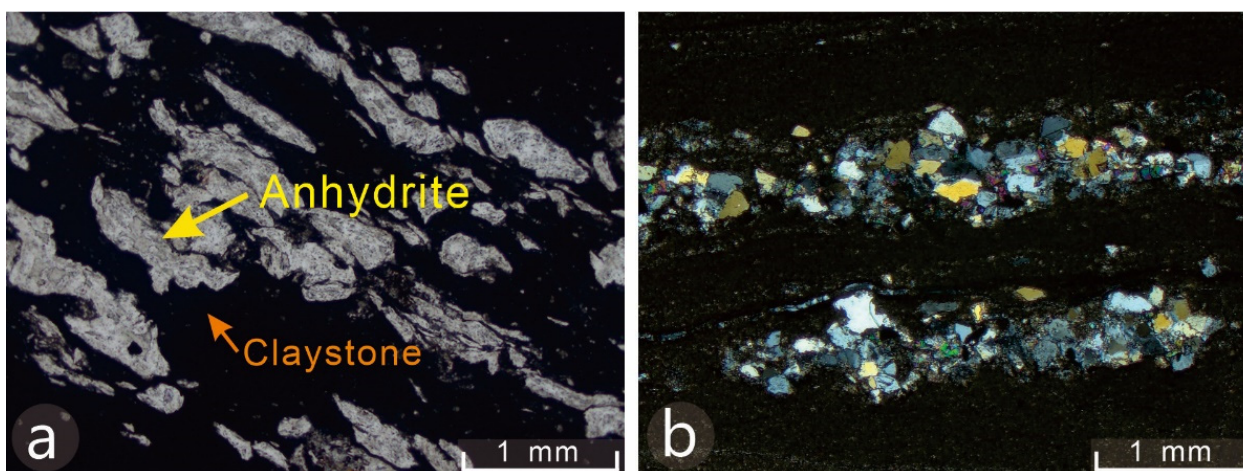


**Figure 7.** Typical Lower–Middle Cambrian claystones from outcrops and cores. (a) Anhydrite claystone, thin section (transmitted light), Awatag Fm., well YH10 (6212 m); (b) siliceous claystone, thin section (crossed polars), Wusongger Fm., well BT5 (5647 m).

#### 4.2. Organic Matter Content

The TOC analysis results of 54 samples from well H4 and 56 samples from well ZS1 show that TOC ranges from 0 to 7.06% and averages 0.66%. Specifically, the TOC ranges from 0.11% to 7.06% and averages 0.85% in the Awatag Fm., from 0.1% to 1.85% and averages 0.46% in the Shayilik Fm., from 0 to 2.32% and averages 0.5% in the Wusongger Fm., and from 0.17% to 1.18% and averages 0.41% in the Xiaerbrak Fm. (Tables 1 and 2). The data from the 54 pyrolysis samples from well H4 show that the  $S_1+S_2$  ranges from 0.07 to 105.34 mg/g and averages 2.68 mg/g. Specifically, the  $S_1+S_2$  ranges from 0.15 to 105.34 mg/g and averages 4.79 in the Awatag Fm., from 0.28 to 0.85 mg/g and averages 0.48 in the Shayilik Fm., from 0.07 to 4.43 mg/g and averages 0.48 in the Wusongger Fm., and from 0.12 to 1.77 mg/g and averages 0.52 in the Xiaerbrak Fm. The result indicates a relatively low content of organic matter in the Lower–Middle Cambrian evaporite series.

As shown in Figure 4, there is an obvious positive correlation between the TOC and the  $S_1+S_2$  of the platform source rocks of the Lower–Middle Cambrian evaporite series in the Tarim basin, indicating that the higher the TOC of the shallow water source rocks, the greater the hydrocarbon generation potential. According to the evaluation criteria of marine carbonate source rocks [37–39], rocks with TOC values less than 0.5% are ineffective source rocks, accounting for 65% of sampled formations from this study. Those with TOC values between 0.5% and 1% are poor source rocks, and those with TOC values between 1% and 2% are fair source rocks, accounting for 10% of sampled formations. Finally, those with TOC values greater than 2% are good source rocks, accounting for 5% (Figure 8) of sampled formations. In the Awatag Fm., 37% of the TOC values are greater than 0.5%; 14% are poor source rocks, 16% are fair source rocks, and 7% are good source rocks. In the Shayilik Fm., 25% of the TOC values are greater than 0.5%; 17% are poor source rocks and 8% are fair source rocks. In the Wusongger Fm., 37% of the TOC values are greater than 0.5%; 33% are poor source rocks and 4% are good source rocks. In the Xiaerbrak Fm., 28% of the TOC values are greater than 0.5%; 22% are poor source rocks and 6% are fair source rocks.

#### 4.3. Organic Matter Type

Fifty-four pyrolysis datapoints of well H4 show that the HI of shallow water source rocks ranges from 7 to 227 mg HC/g TOC and averages 78 mg HC/g TOC. Specifically, in the Awatag Fm., the HI ranges from 46 to 227 mg HC/g TOC and averages 110 mg HC/g TOC. In the Shayilik Fm., HI ranges from 56 to 64 mg HC/g TOC and averages 61 mg HC/g TOC. In the Wusongger Fm., the HI ranges from 7 to 108 mg HC/g TOC and averages 31 mg HC/g TOC. In the Xiaerbrak Fm., the HI ranges from 29 to 108 mg HC/g TOC and averages 60 mg HC/g TOC. The  $T_{max}$  ranges from 394 °C to 607 °C and

averages 434 °C. In detail, the Tmax ranges from 403 °C to 445 °C and averages 424 °C in the Awatag Fm., from 412 °C to 431 °C and averages 423 °C in the Shayilik Fm, from 394 °C to 607 °C and averages 481 °C in the Wusongger Fm., and from 396 °C to 416 °C and averages 410 °C in the Xiaoerbrak Fm. (Table 1). The plot of HI versus Tmax can be used to classify the type of organic matter [40], and it shows that the kerogen in most samples of the Lower–Middle Cambrian evaporite series is predominantly Type III; only six samples were Type II (Figure 9).

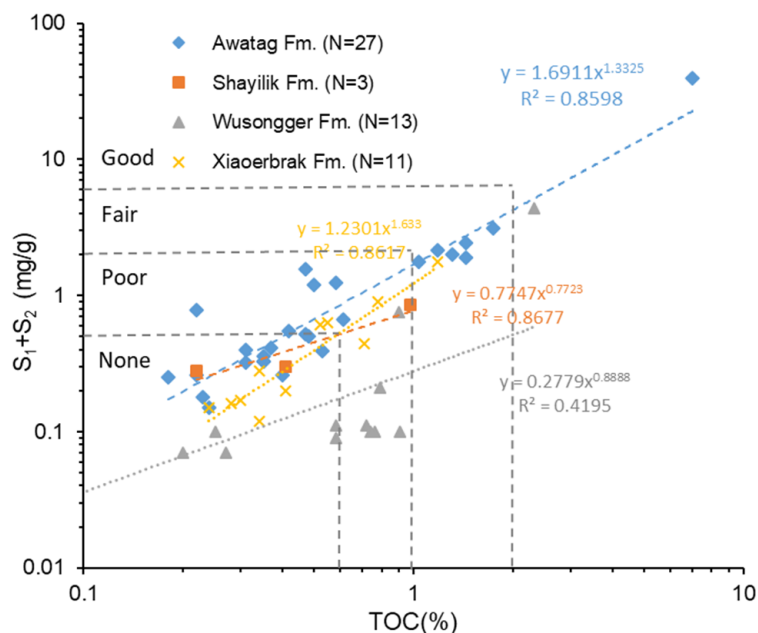


**Figure 8.** TOC versus (S<sub>1</sub> + S<sub>2</sub>) plot showing that the Lower–Middle Cambrian shallow water source rocks in the evaporite series are mainly fair–poor source rocks (maturation scale from ref [37]). N = number of samples.

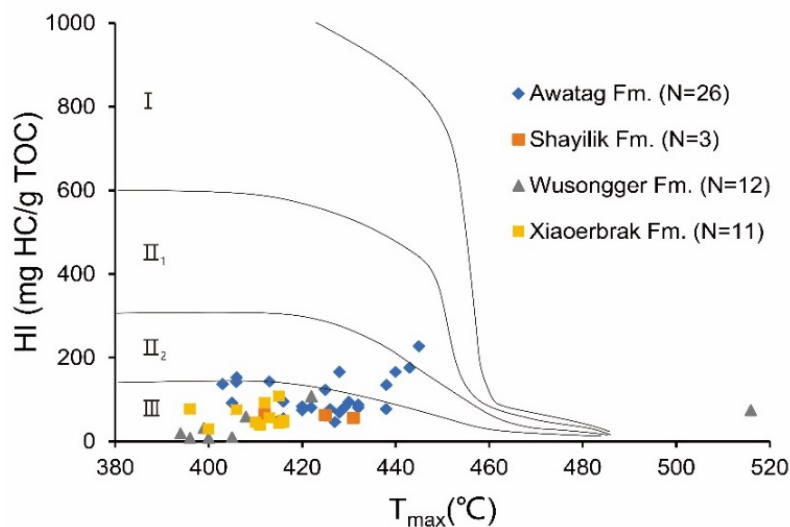


**Figure 9.** Hydrogen index (HI) versus Tmax plot showing the kerogen type of the Lower–Middle Cambrian evaporite series in Tarim Basin (maturation scale from ref. [40]). N = number of samples.

Plots of S<sub>2</sub> versus TOC can also be used to study the organic matter type. As the data show, the S<sub>2</sub> ranges from 0.05 to 66.04 mg HC/g rock and averages 1.73 mg HC/g rock. In detail, the S<sub>2</sub> ranges from 0.11 to 66.04 mg HC/g rock and averages 3.14 mg HC/g rock

in the Awatag Fm., from 0.14 to 0.62 mg HC/g rock and averages 0.33 mg HC/g rock in the Shayilik Fm., from 0.05 to 2.51 mg HC/g rock and averages 0.3 mg HC/g rock in the Wusongger Fm., and from 0.1 to 1.27 mg HC/g rock and averages 0.36 mg HC/g rock in the Xiaoerbrak Fm. (Table 1). The TOC and  $S_2$  are positively correlated in all of the four formations, and the fitting coefficients  $R^2$  were 0.8971, 0.7957, 0.9957, and 0.9397 from the Xiaoerbrak Fm. to the Awatag Fm. As the plot of  $S_2$  versus TOC shows, most of the organic matter is dominated by Type III kerogen but with minor Type I and Type II in the Wusongger Fm (Figure 10).

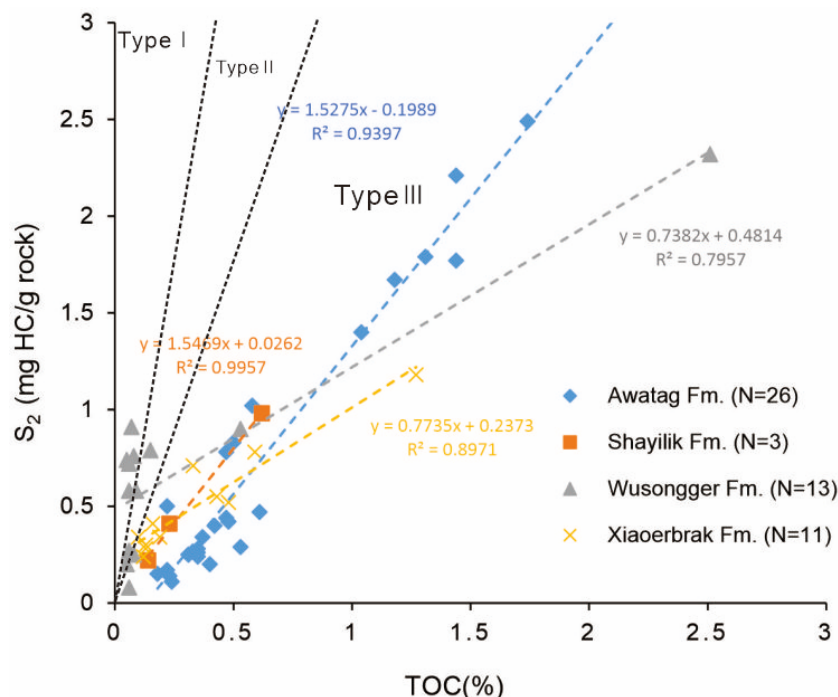


**Figure 10.** TOC versus  $S_2$  plot showing the kerogen types of the Lower–Middle Cambrian evaporite series in Tarim Basin (maturation scale from ref [41]). N = number of samples.

#### 4.4. Major Elements

The major element results of the Lower–Middle Cambrian of well ZS1 are shown in Table 2 and Figure 11. The aluminum trioxide ( $Al_2O_3$ ) ranges from 0 to 5.98% and averages 0.79%. In detail, the  $Al_2O_3$  in the Xiaoerbrak Fm. has the highest value, which ranges from 0.04% to 5.98% and averages 2.66%. Next is the  $Al_2O_3$  in the Wusongger Fm., which ranges from 0.18% to 1.59% and averages 0.83%. Then, the  $Al_2O_3$  values in the Awatag Fm. range from 0.02% to 1.95% and average 0.46% and the  $Al_2O_3$  in the Shayilik Fm. has the lowest and most stable values, ranging from 0 to 0.12% and averaging 0.07%. The magnesium oxide (MgO) ranges from 11.18% to 22.45% and averages 19.54%. However, the trend of the MgO is just the opposite of that of the  $Al_2O_3$ . The MgO values in the Shayilik Fm. are the highest, ranging from 21.44% to 22.45% and averaging 22.12%. Next is the MgO in the Awatag Fm., which ranges from 15.11% to 22.38% and averages 19.36%. Then, MgO ranges from 11.18% to 20.26% and averages 18.42% in the Wusongger Fm. The lowest value is in the Xiaoerbrak Fm., which ranges from 13.31% to 21.37% and averages 18.22%. The trend of the calcium oxide (CaO) is similar to that of the MgO. The average values from the Xiaoerbrak Fm. to the Awatag Fm. are 24.39%, 26.9%, 29.68%, and 27.26%.

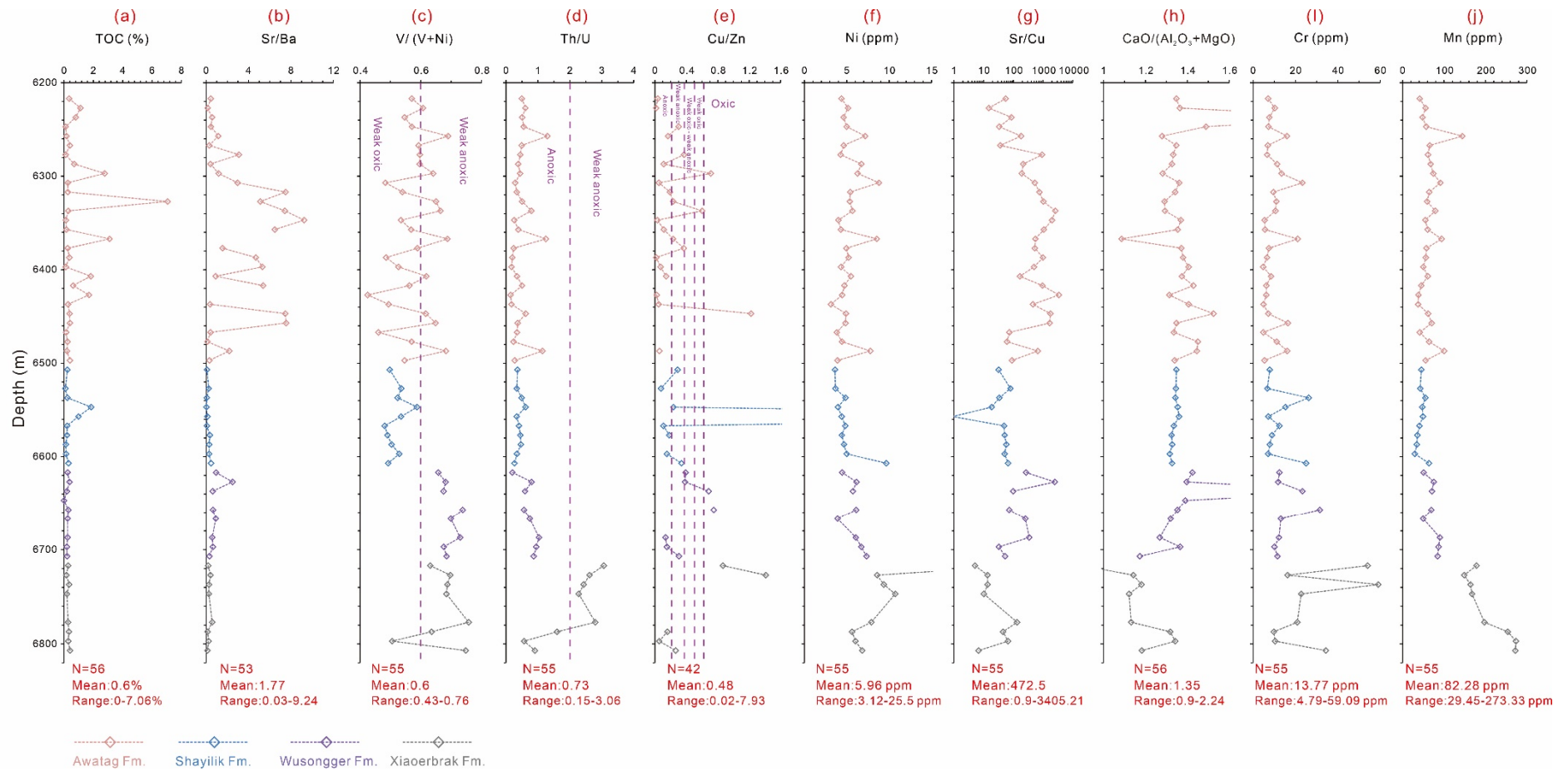


**Figure 11.** Geochemical data versus depth of the Lower–Middle Cambrian shallow water source rocks in the evaporite series, Tarim Basin: (a) TOC versus depth; (b) Sr/Ba ratio versus depth; (c) V/(V+Ni) ratio versus depth; (d) Th/U versus depth; (e) Cu/Zn versus depth; (f) nickel (Ni) versus depth; (g) Sr/Cu versus depth; (h) CaO (Al<sub>2</sub>O<sub>3</sub> + MgO) versus depth; (i) chromium (Cr) versus depth; (j) manganese (Mn) versus depth. N = number of samples.

#### 4.5. Trace Elements

The measurement results of the trace elements, including V, Cr, Mn, Ni, Cu, Zn, Sr, Ba, Th, and U, are shown in Table 2 and Figure 11. On average, element content data show that the most abundant trace elements in the shallow water source rocks of the Lower–Middle Cambrian evaporite series are Sr (1295 ppm), Ba (957.46 ppm), Mn (82.28 ppm), Zn (34.25 ppm), Cr (13.77 ppm), and V (10.46 ppm). The concentrations of other trace elements are lower than 10 ppm; for example, Ni (5.96 ppm), Cu (5.03 ppm), U (1.35 ppm), and Th (1.05 ppm). All the elements vary significantly with increasing burial depth. V, Mn, Ni, and Th share a similar trend; these elements present the highest concentration values in the Xiaoerbrak Fm. and the lowest values in the Shayilik Fm. Cr is only a little different from the last four elements in that the lowest value is in the Awatag Fm. The concentrations of Sr, Zn, and U in the Awatag Fm. and the Wusongger Fm. are higher than those in the Shayilik Fm. and the Xiaoerbrak Fm. However, the trend of Cu is the opposite; the concentrations of Cu in the Awatag Fm. and the Wusongger Fm. are lower than that in the Shayilik Fm. and the Xiaoerbrak Fm. When it comes to Ba, the concentrations in the Wusongger Fm. and the Shayilik Fm. are much higher than that in the Awatag Fm. and the Xiaoerbrak Fm.

The Sr/Ba ratio and the Sr/Cu ratio in the Awatag Fm. are the highest and the most unstable values in the four formations. The Cu/Zn ratio, on the contrary, is higher in the Shayilik Fm. and the Xiaoerbrak Fm. than in the other two formations. The V/(V+Ni) ratio and the Th/U ratio are both higher in the Lower Cambrian than in the Middle Cambrian.

### 5. Discussion

#### 5.1. Lithologies, Facies, and their Meaning in the Paleoenvironment

In a broad sense, the term “evaporite” refers to rocks of chemical origin, including halite deposits, gypsum, and some carbonates, which are driven by solar evaporation and gradually condense brine to saturation, so that different salts crystallize according to their solubility [42,43]. The evaporite series mentioned in this paper refers to a series of sedimentary units that formed in a restricted area during times of increasing salinity on the platform, whereas coeval claystones and other carbonate rocks of the same age formed on the outer, less restricted platform areas and on the slope.

Gypsum and halite are usually precipitated from high-salinity brine under arid climate conditions. Gypsum can be converted into anhydrite by dehydration during burial diagenesis. For facies, the evaporite sediments usually correspond to the evaporitic platform, which is developed in the Wusongger Fm. and the Awatag Fm. However, in addition to evaporites, evaporitic platform deposits also include claystones, carbonates, and the interbedded assemblages made up of them. Just like the anhydrite claystones and dolomitic claystones, the mixture of claystones, carbonates, and evaporites are formed during periods of fluctuation of seawater in the evaporitic platform. Claystone deposits are developed in the short deep water stage during the evaporitic platform period, which begins to precipitate carbonate and gypsum, with seawater becoming shallower and saltier. As a result, claystones mixed with carbonate and gypsum were formed. In the process of burial diagenesis, calcite gradually evolved into dolomite, and gypsum gradually evolved into anhydrite and finally formed dolomitic claystone and anhydrite claystone.

Stromatolite dolomite and grain dolomite are usually the main components of microbial reefs and shoals. Considering the palaeogeographic pattern of the Early Middle Cambrian in the Tarim Basin, the microbial reefs and shoals in the North Tarim Uplift and the East Tarim Uplift should be platform margin sediments, while those in the Central Tarim Uplift and the Bachu Uplift are intra-platform deposits. The development of intra-platform microbial reefs and shoals without evaporite deposits shows that the platform is a restricted platform with a semi-closed hydrological cycle to the open ocean. The upper part of the Xiaoerbrak Fm. (Figures 2 and 3) is a typical example. Similarly, without intra-platform microbial reefs, shoals, and evaporite deposits, the platform is an open

platform with an open water cycle. This corresponds to the lower part of the Xiaerbrak Fm. of well H4 (Figure 2) and well ZS1 (Figure 3).

Generally speaking, since the formation of the platform within the Xiaerbrak Fm., the study area has experienced two evolutionary cycles from open platform to restricted platform and evaporitic platform. The hydrological cycle between the platform area and the open ocean has also undergone an evolution from open to closed. The fluctuations of the paleo-sea level during the evaporitic platform period lead to the hydrological cycle's instability, which further leads to the interbedding of evaporites, carbonates, and claystones.

### 5.2. Paleosalinity and Its Implication for Organic Matter Enrichment of Shallow Water Evaporitic Environment

Previous studies show that salinized lakes or salinized lagoons are beneficial to the accumulation of organic matter and hydrocarbon source rocks [11,42,43]. Generally, the Sr/Ba ratio in seawater positively correlates to the water salinity [41,44,45]. Therefore, it is used to analyze the paleosalinity of the shallow water environment of the platform area during the Early and Middle Cambrian.

As Figure 12a shows, the Sr/Ba ratio and TOC show no correlation in the Awatag Fm. with an  $R^2$  of 0.0002 and a strong positive correlation in the Wusongger Fm., with an  $R^2$  of 0.7098. Their sedimentary facies are evaporitic platforms (Figure 3). However, the correlations are negative in the Shayilik Fm. with an  $R^2$  of 0.2094 and the Xiaerbrak Fm., with an  $R^2$  of 0.2846. The sedimentary facies developed in the Shayilik Fm. and the Xiaerbrak Fm. are restricted platforms and open platforms, which reflect lower salinity (Figure 11b). There is also a clear partition in the Awatag Fm. (Figure 12b). When the Sr/Ba ratio  $<1.2$ , the TOC increases rapidly with the increase in the Sr/Ba ratio, with an  $R^2$  of 0.6778, while when the Sr/Ba ratio  $>1.2$ , the TOC increases slowly with the increase in the Sr/Ba ratio, with an  $R^2$  of 0.0138. This indicates that shallow water source rocks can effectively accumulate organic matter only in a seawater environment with appropriate salinity. When the paleosalinity is so low as to deposit only carbonates, such as the carbonate layers of the Xiaerbrak Fm. and the Shayilik Fm., the TOC value is negatively correlated with the salinity. When the paleosalinity is high enough to deposit only thick layers of evaporites, for example, the thick layers of halites or anhydrite in the Wusongger Fm. and the Awatag Fm., the TOC value can be as low as 0 (Figure 2, Figure 3, and a and Tables 1 and 2). Only when the paleosalinity is between them is the TOC value proportional to the salinity.

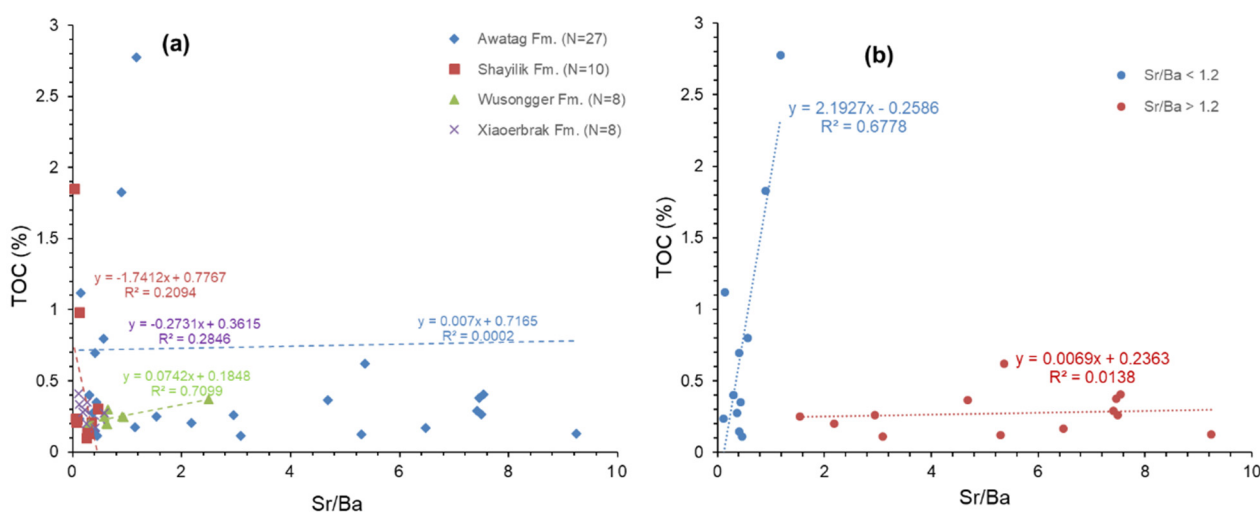


**Figure 12.** Correlation between Sr/Ba ratio and TOC content of the Lower–Middle Cambrian shallow water source rocks in the evaporite series, Tarim Basin. (a) Samples from all the four formations; (b) samples from the Awatag Fm. N = number of samples.

### 5.3. Redox Proxies and Its Implication for Organic Matter Enrichment of Shallow Water Evaporitic Environment

The V/(V+Ni) ratio can be used as an index to study the redox properties. The larger the V/(V+Ni) ratio is, the stronger the reducibility of the sedimentary environment. V/(V+Ni) ratio ranges between 0.84 and 1, 0.6 and 0.84, 0.43 and 0.6, and less than 0.43 correspond to anoxic, weak anoxic, weak oxic, and oxygen-rich sedimentary environments, respectively [44,46]. As shown in Figures 11c and 13a, the V/(V+Ni) ratio of 56 samples from well ZS1 is generally greater than 0.43 and less than 0.84, suggesting that the platform area was generally in a weak oxic to weak anoxic environment during the deposition of the Lower–Middle Cambrian evaporite series in the Tarim Basin. Most of the samples in the Xiaoerbrak Fm. and the Wusongger Fm. have V/(V+Ni) ratios greater than 0.6, suggesting that they were developed in a weak anoxic environment (Figure 11c). The Shayilik Fm. was developed in a weak oxic environment because all the V/(V+Ni) ratios of the samples in this formation are less than 0.6. The Awatag Fm. shows alternating oscillations of weak oxic and weak anoxic environments because the V/(V+Ni) ratios of the 29 samples fluctuate around 0.6. Comparatively, the redox conditions of the Xiaoerbrak Fm. and the Wusongger Fm. have a higher level of anoxia than the upper two formations, but the redox conditions of the Awatag Fm. vary more than the other formations, suggesting stronger heterogeneity. There is a positive correlation between the TOC and the V/(V+Ni) ratio in the Lower–Middle Cambrian evaporite series (Figure 13a). The fitting coefficients  $R^2$  are 0.0907 in the Awatag Fm., 0.6111 in the Shayilik Fm., 0.0734 in the Wusongger Fm., and 0.0038 in the Xiaoerbrak Fm. However, there is also a relatively obvious regionalization. While some of the samples with high TOC values in the Awatag Fm. and the Shayilik Fm. have a strong positive correlation with the V/(V+Ni) ratios, the others have a relatively weak positive correlation (Figure 13a).

The Th/U ratio is another index of redox conditions. A Th/U ratio between 0 and 2 represents an anoxic environment, a Th/U ratio between 2 and 8 represents an oxygen-lean environment, and a Th/U ratio greater than 8 represents an oxic environment [47,48]. As shown in Figure 11d, except for few of the samples from the Xiaoerbrak Fm. where the Th/U ratio is greater than 2, all the other data show Th/U ratios that are less than 1 or just around 1, suggesting that the Lower–Middle Cambrian evaporite series were mostly deposited in an anoxic environment and that only a small portion of the Xiaoerbrak Fm. was formed in an oxygen-lean environment. The correlation analysis between TOC values and Th/U ratios shows positive correlations in the Awatag Fm. and the Shayilik Fm., and negative correlations in the Wusongger Fm. and the Xiaoerbrak Fm. As far as the redox index is concerned, the indicative meaning of the Th/U ratio is slightly different from that of the V/(V+Ni) ratio, but it also shows that there are obvious differences between the Middle Cambrian and the Lower Cambrian (Figure 13a,b).

The Cu/Zn ratio is another index of redox conditions; the lower the ratio is, the more anoxic the environment. A Cu/Zn ratio less than 0.21 represents an anoxic environment, a Cu/Zn ratio between 0.21 and 0.38 represents a weak anoxic environment, a Cu/Zn ratio between 0.38 and 0.5 represents a transition from a weak anoxic to a weak oxic environment, a Cu/Zn ratio between 0.5 and 0.63, represents a weak oxic environment, and a Cu/Zn ratio greater than 0.63 represents a relatively oxic environment. As shown in Figures 11e and 13c, the evaporite series in the platform area represented by the well ZS1 were generally deposited in an anoxic to weak anoxic environment, except small portions of the Wusongger Fm. and the Xiaoerbrak Fm. which were deposited in a relatively oxic environment. In terms of the correlation between the Cu/Zn ratio and TOC, only the Xiaoerbrak Fm. shows a weak negative correlation, while the other formations show weak positive correlations.

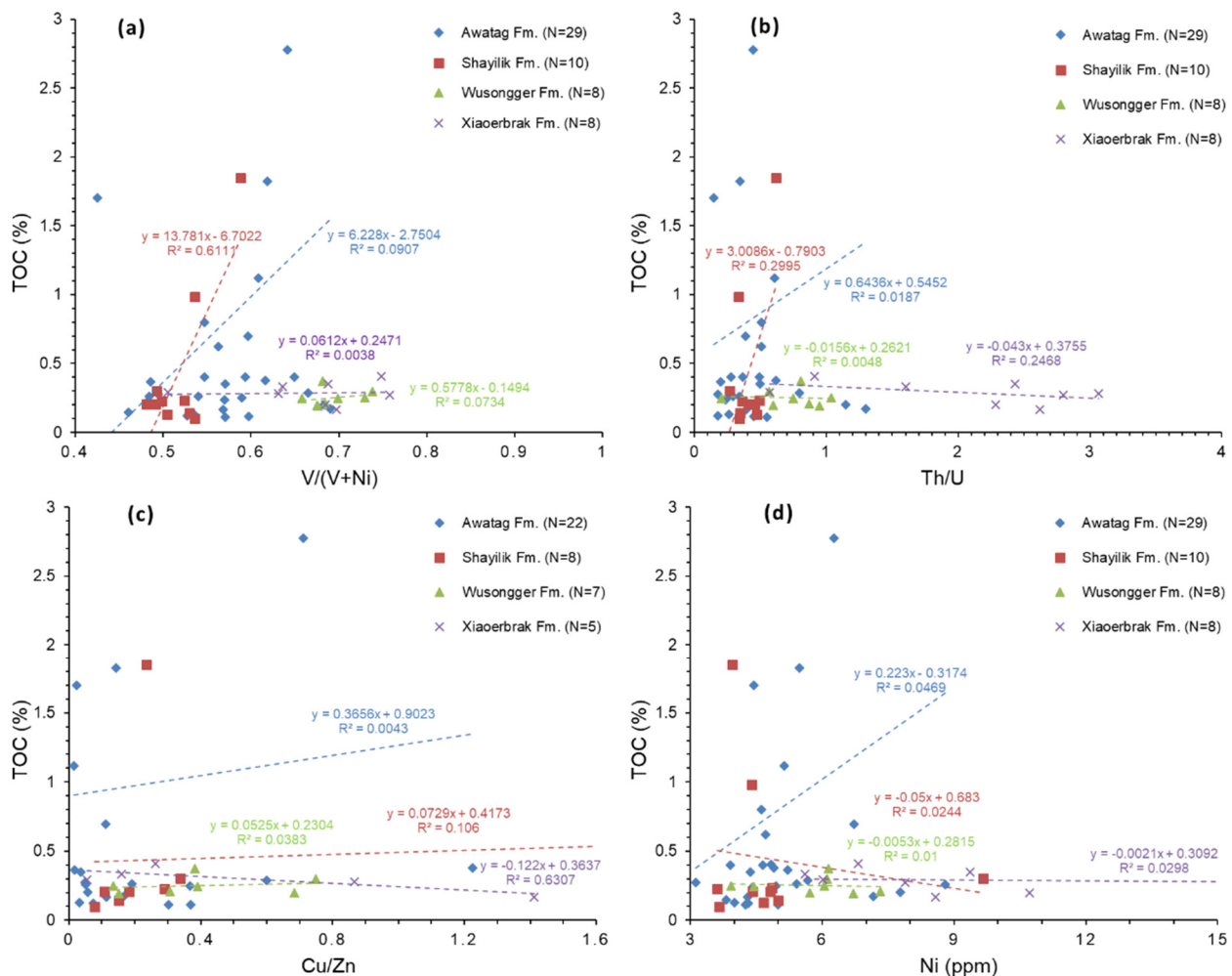


**Figure 13.** Correlation between redox parameters and TOC content of the Lower–Middle Cambrian shallow water source rocks in the evaporite series, Tarim Basin. (a) V/(V+Ni) ratio versus TOC; (b) Th/U ratio versus TOC; (c) Cu/Zn ratio versus TOC; (d) nickel (Ni) versus TOC. N = number of samples.

There are some slight differences between the three methods above. The V/(V+Ni) ratio analysis indicates that the Xiaoerbrak Fm. and the Wusongger Fm. were developed in a weak anoxic environment, the Shayilik Fm. was developed in a weak oxic environment, and the Awatag Fm. was developed in an environment with weak oxic and weak anoxic reciprocating changes. The Th/U ratio analysis indicates that they were mostly deposited in an anoxic environment and that only a small portion of the Xiaoerbrak Fm. was formed in an oxygen-lean environment. Finally, the Cu/Zn ratio analysis indicates that most of them were deposited in an anoxic to weak anoxic environment, except a small portion of the Wusongger Fm. and the Xiaoerbrak Fm., which were developed in an oxic environment. The contradictions may be caused by the different evaluation criteria of previous studies on other basins or just by the different number of samples in each method. However, all the indexes of redox conditions show that most of the shallow water source rocks of the Lower–Middle Cambrian were deposited in a weak oxic to weak anoxic or anoxic environment, and most of them suggest a weak positive correlation between redox conditions and TOC.

#### 5.4. Paleoproductivity and Its Implication for Organic Matter Enrichment of Shallow Water Evaporitic Environment

Paleoproductivity is a very important parameter to evaluate the organic matter enrichment of source rocks [41,49]. Ni can be accumulated gradually during the decomposition of organic matter, so it can be used as an important index to reflect the surface productivity

of ancient seawater. The higher the content of Ni, the higher the paleoproductivity of the surface seawater [41]. As shown in Figures 11f and 13d, the Ni contents in the Xiaerbrak Fm. are the highest in the Lower–Middle Cambrian evaporite series in the Tarim Basin, with an average value of 10.06 ppm. The Ni contents in the Wusongger Fm. are the second highest, with an average value of 5.8 ppm. The Ni contents in the Shayilik Fm. are the lowest, with an average of 4.8 ppm. Just like the previous indexes, there is an obvious partition of the Ni contents in the Awatag Fm. The samples with TOC values greater than 0.5 have Ni contents less than 7 ppm, and the TOC values increase rapidly with the Ni content, while the samples with Ni contents greater than 7 ppm only have very low TOC. However, further analysis indicates that the correlation between TOC and Ni contents is only weakly positive in the Awatag Fm., with an  $R^2$  of 0.0469, while the correlations in the other formations are all weakly negative (Figure 13d). As the analysis showed, the paleoproductivity is only beneficial to the enrichment of organic matter in some parts of the Awatag Fm.

### 5.5. Paleoclimate and Its Implication for Organic Matter Enrichment of Shallow Water Evaporitic Environment

The Sr/Cu ratio is an index commonly used in paleoclimate studies [47]. The higher the Sr/Cu ratio, the dryer the paleoclimate. Ratios of Sr/Cu ranging between 1.3 and 5 represent a humid climate; ratios of Sr/Cu greater than 5 represent a dry and hot climate [47]. As shown in Table 2 and Figure 11g, all the Sr/Cu ratios of the samples from well ZS1 are greater than 5, suggesting that all the Lower–Middle Cambrian shallow water source rocks were developed in a dry and hot environment. In detail, the Sr/Cu ratios have the highest values in the Awatag Fm., with an average of 746. The second highest values are in the Wusongger Fm., with an average of 451, and the lowest values are in the Shayilik Fm. and the Xiaerbrak Fm., with average values of 43 and 36. Comparatively, the paleoclimate of the Awatag Fm. and the Wusongger Fm. during sedimentation was much dryer and hotter than that of the Shayilik Fm. and the Xiaerbrak Fm. Further analysis of the correlation between the TOC and the Sr/Cu ratios indicates that the correlation is only negative in the Shayilik Fm., but weakly positive in the other formations (Figure 14a).

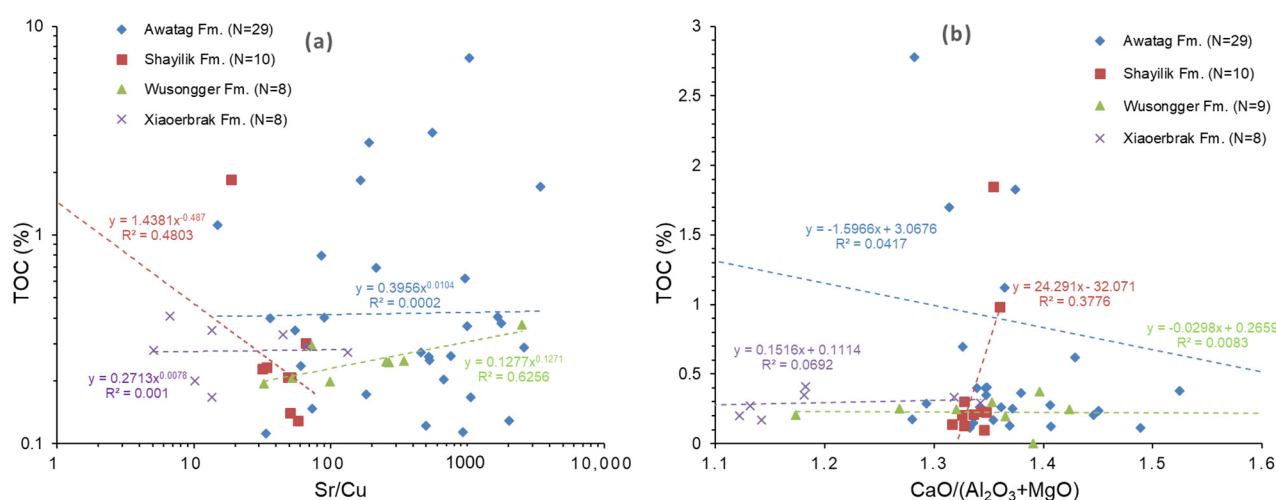


**Figure 14.** Correlation between paleoclimate parameters and TOC content of the Lower–Middle Cambrian shallow water source rocks in the evaporite series, Tarim Basin. (a) Sr/Cu ratio versus TOC; (b) CaO/(Al<sub>2</sub>O<sub>3</sub>+MgO) ratio versus TOC. N = number of samples.

The CaO/(Al<sub>2</sub>O<sub>3</sub>+MgO) ratio is another index used to evaluate paleoclimate. The smaller the CaO/(Al<sub>2</sub>O<sub>3</sub>+MgO) ratio, the wetter and cooler the climate; on the contrary, the drier and hotter the climate [48]. According to Table 2, Figure 11h, and Figure 14b, the CaO/(Al<sub>2</sub>O<sub>3</sub> + MgO) ratios are higher in the Awatag Fm. and the Wusongger Fm., with

average values of 1.39 and 1.44, than in the Shayilik Fm. and the Xiaoerbrak Fm., with average values of 1.34 and 1.16. This indicates that the paleoclimate in the Awatag Fm. and the Wusongger Fm. was dryer and hotter than the other formations during sedimentation. The correlation between the  $\text{CaO}/(\text{Al}_2\text{O}_3 + \text{MgO})$  ratio and TOC is positive in the Shayilik Fm. and the Xiaoerbrak Fm. and negative in the other two formations.

The comparison of multi-parameters does not seem to prove the direct influence of paleoclimate conditions on the enrichment of organic matter in shallow water source rocks, but it can be seen from the statistical data (Table 2 and Figure 11) that the indexes reflecting paleoclimate change correspond to the evolution of sedimentary facies. The dry and hot climate corresponds to the evaporitic platform, while the relatively warm and humid climate corresponds to the open platform.

### 5.6. Paleo-Seawater Depth and Its Implication for Organic Matter Enrichment of Shallow Water Evaporitic Environment

The Cr content is important index to evaluate the paleo-seawater depth since Cr is mainly adsorbed on clay minerals, and its content increases with the increase in seawater depth and distance from the coast [50]. Therefore, the content of Cr has a positive correlation with the paleo-seawater depth. As shown in Table 2 and Figure 11i, the Cr content decreases gradually from the Xiaoerbrak Fm. to the Awatag Fm., with average values of 28.45 ppm, 15.75 ppm, 12.47 ppm, and 9.62 ppm, respectively. This suggests that the platform area of the Tarim Basin became shallower throughout the Early and Middle Cambrian. Just like the Mn content, the correlations between Cr content and TOC are mainly positive but not that obvious because the fitting coefficient  $R^2$  values are all very small (Figure 15a).

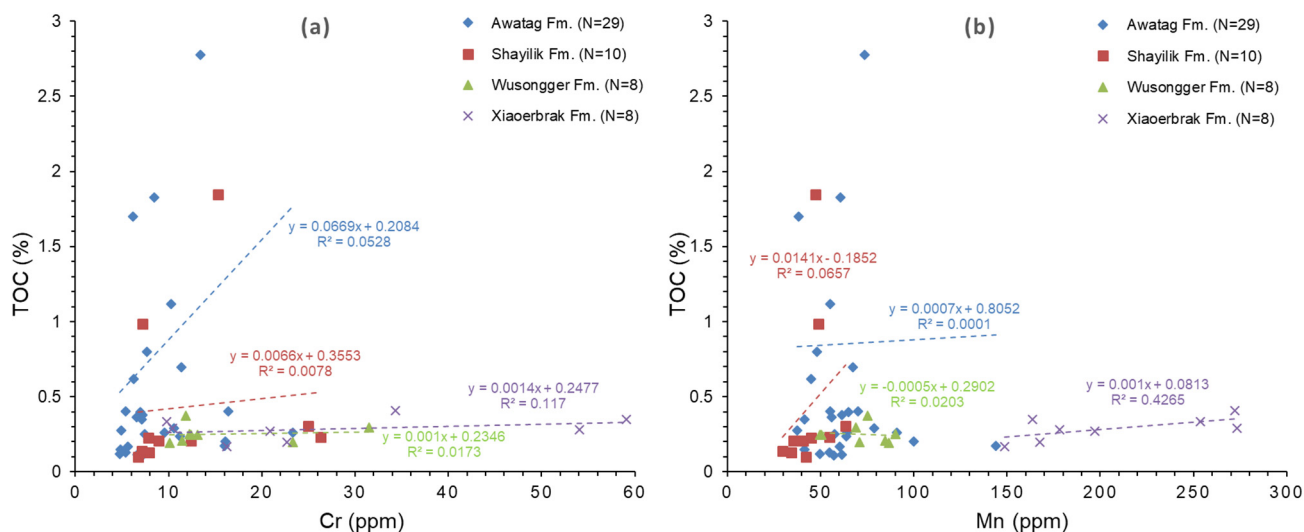


**Figure 15.** Correlation between paleo-seawater depth parameters and TOC content of the Lower–Middle Cambrian shallow water source rocks in the evaporite series, Tarim Basin. (a) Chromium (Cr) versus TOC; (b) manganese (Mn) versus TOC. N = number of samples.

Previous studies [44,50,51] have shown that Mn can stably exist in ionic solutions, so in the seawater environment, Mn is more likely to be enriched in the still water seafloor far from the coast. Therefore, the content of Mn in marine mudstone, shale, and micritic limestone is used as an index to analyze the distance from the coast or the depth of paleo-sea water. The greater the Mn content, the greater the depth of the paleo-seawater [44]. As shown in Table 2 and Figure 11j, the Mn content is the highest in the Xiaoerbrak Fm., with an average value of 206.84 ppm, while the contents in the Wusongger Fm., the Shayilik Fm., and the Awatag Fm. have average values of 72.06 ppm, 44.21 ppm, and 63.87 ppm, respectively. TOC and Mn content have a weakly positive correlation in all of the four formations but with very small fitting coefficient  $R^2$  values (Figure 15b). As shown in

Figure 15a,b, although the correlation between the TOC values and the contents of Mn and Cr in each formation is not ideal, it can be seen that the samples with TOC values greater than 0.5% have lower contents of Mn and Cr, while the samples with higher contents of Mn and Cr have TOC values lower than 0.5%. This shows that the enrichment of organic matter in shallow water source rocks only occurs in a certain paleo-seawater depth.

#### *5.7. Factors Controlling Organic Matter Enrichment and Its Implications for Organic-Rich Source Rock Prediction*

Generally, paleosalinity, redox condition, paleoproductivity, paleoclimate, and paleo-seawater depth all influence the enrichment of organic matter in shallow water source rocks of the Lower–Middle Cambrian evaporite series in the Tarim Basin. In detail, paleosalinity and paleo-seawater depth need to be within a certain range in order to facilitate the accumulation of organic matter in shallow water source rocks, so they are the main controlling factors. The parameters reflecting the redox conditions show that the evaporite series in the platform area was mainly developed in a weak anoxic sedimentary environment, so the redox conditions have no obvious effect on organic matter enrichment. Paleoclimate does not directly control the enrichment of organic matter but corresponds to the development of sedimentary facies. The correlation between paleoproductivity and organic matter enrichment seems to be valid only in Awatag Fm., indicating that paleoproductivity is indeed the controlling factor of organic matter enrichment but not a direct factor. Therefore, the total evidence seems to suggest that the formation of the shallow water source rocks with high TOC values in the Awatag Fm. benefits from the weak anoxic environment of the unstable paleosalinity and paleo-seawater depth of the evaporitic platform in the dry and hot paleoclimate, in which the paleoproductivity promotes the accumulation of organic matter. Thus, the exploration of hydrocarbon source rocks in the Lower–Middle Cambrian in the Tarim Basin should also focus on the shallow water source rocks in the evaporitic platform, developed in the environment of appropriate salinity, weak anoxia, and moderate paleo-seawater depth. Such an environment is usually formed in the unstable period of platform water, so the target of shallow water source rocks can be selected with the interbedded layers of evaporites, carbonates, and claystones, like the evaporite series in the Awatag Fm. in the Tarim Basin.

According to these results, the platform source rocks probably formed in a period characterized by high-frequency sea-level fluctuations. They are common in the lower parts of the Wusongger Formation and Awatag Formation. Taking well H4 as an example (Figure 2), the upper part of the Wusongger Formation was deposited during a stable period of very high salinity, and the thick continuous halite inhibited the formation of platform source rocks such as anhydrite claystone and dolomitic claystone. In contrast, during the deposition of the Shayilik Formation, a large amount of limestone formed, indicating more or less normal marine conditions on the platform. Due to the well-oxygenated water, most of the produced organic matter was decomposed on the seafloor, and thus the TOC content of the sediments did not increase. During the deposition of the lower part of Wusongger and Awatag Formations, however, rapidly changing lithologies of halite, gypsum, and claystone, including dolomitic claystone and gypsum claystone, indicate minor but high-frequency sea-level fluctuations. Probably, during short-term rises, low-TOC limestones formed in well-oxygenated, more or less normal marine water (Figure 16a). Later, with ongoing restriction of the platform and reduced water exchange, a salinity-stratified water body developed on the platform with well-oxygenated surface water but less oxygenated or even anoxic bottom water. Organic matter produced in the surface water was only incompletely decomposed in the strongly stratified water body, resulting in the formation of TOC-rich but carbonate-poor shallow platform source rocks lacking evidence of benthic life (Figure 16b). The overall salinity of the platform water during these times was probably elevated but not high enough for evaporation. The uppermost part of the water bodies contained sufficient free oxygen and evaporation led to relatively high salinity, which was suitable for the survival of aerobic halophilic algae and zooplankton. Deposits from such settings are often characterized by high TOC contents resulting from abundant halophilic

algae microorganisms and thus can form hydrocarbon source rocks [5,11,12]. The late stages of these cycles are characterized by very shallow conditions and very high salinity, resulting in the formation of evaporites (Figure 16c). These evaporites have very low TOC content because the salinity was too high for planktic production. During the late stage of the Awatag Formation, evaporative conditions persisted for a long time, and the deposition of thick monotonous halites suppressed the formation of shallow platform source rocks.

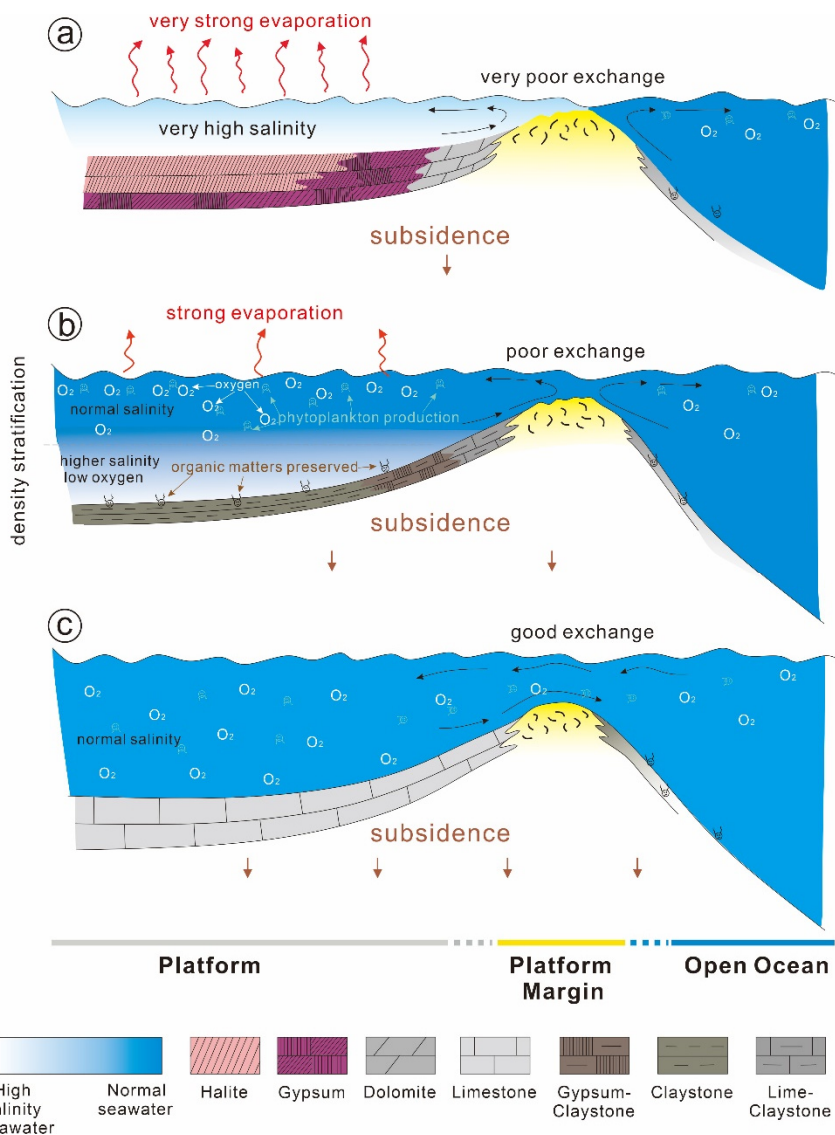


**Figure 16.** Models of the formation of the three main lithologies on the platform. During stage b, the shallow water source rocks formed. (a) very poor exchange; (b) poor exchange; (c) good exchange.

**6. Conclusions**

Based on the analyses of geochemical parameters for the accumulation of organic matter of the Lower–Middle Cambrian shallow water source rocks in the Tarim Basin, the following conclusions are drawn:

(1) The shallow water source rocks of the Lower–Middle Cambrian evaporite series in the Tarim Basin mainly developed in the Awatag Fm. and the Wusongger Fm., in which 37% of the samples have TOC values greater than 0.5%, which are mainly fair or poor source rocks. The kerogen in the shallowest water source rocks is mainly of Type III.

(2) The enrichment of organic matter first increased and then decreased with the increase in paleosalinity. The platform area of the Tarim Basin was generally in a weak

anoxic to an anoxic environment in the Early and Middle Cambrian. The paleoclimate was dry and hot in the Wusongger Fm. and the Awatag Fm.; it was relatively warm and humid in the Xiaoerbrak Fm. and the Shayilik Fm. The paleo-seawater depth became shallower from the Xiaoerbrak Fm. to the Awatag Fm., but all the samples with high content of organic matter come from the shallower environment. The paleoproductivity has little effect on the enrichment of organic matter, and it is only positively correlated with TOC in the Awatag Fm.

(3) The key factors controlling the enrichment of organic matter in shallow water source rocks are paleosalinity and paleo-seawater depth. Redox conditions, paleoclimate, and paleoproductivity play indirect roles in controlling shallow water source rocks, especially the interbedded layers of evaporites, carbonates, and claystones in the Awatag Fm.

**Author Contributions:** Conceptualization, M.W. and Z.B.; methodology, Z.B.; software, M.W.; validation, M.W. and Z.B.; formal analysis, M.W.; investigation, M.W., W.L., and H.Z.; resources, Z.B.; data curation, M.W.; writing—original draft preparation, M.W. and Z.B.; writing—review and editing, M.W., Z.B., A.M., W.L., G.W.M.H., H.Z., D.Z., Z.L., X.X., K.L., Z.S.; visualization, M.W.; supervision, Z.B., A.M.; project administration, Z.B.; funding acquisition, Z.B. All authors have read and agreed to the published version of the manuscript.

**Funding:** This research was funded by the National Key Research and Development Program of China, grant number 2017YFC0603104 and 2018YFC0604304.

**Data Availability Statement:** Not applicable.

**Acknowledgments:** The authors thank the PetroChina Research Institute of Petroleum Exploration and Development and CNPC Tarim oilfield company for their strong support in drilling cores and data use. The authors also thank the reviewers for their constructive suggestions on the modification and improvement of the manuscript.

**Conflicts of Interest:** The authors declare no conflict of interest.

## References

- Hite, R.J.; Anders, D.E. Chapter 4 Petroleum and Evaporites. In *Developments in Sedimentology*; Melvin, J.L., Ed.; Elsevier: Amsterdam, The Netherlands, 1991; Volume 50, pp. 349–411.
- Pannekoek, A.J. Shallow-water and deep-water evaporite deposition. *Am. J. Sci.* **1965**, *263*, 284–285. [[CrossRef](#)]
- Schmalz, R. Deep-Water Evaporite Deposition: A Genetic Model. *Am. Assoc. Pet. Geol. Bull.* **1969**, *53*, 798–823.
- Moody, J.D. *Distribution and Geological Characteristics of Giant Oil Fields. Petroleum and Global Tectonics*; Princeton University Press: Princeton, NJ, USA, 1975; pp. 307–320.
- Warren, J.K. Shallow-water evaporitic environments and their source rock potential. *J. Sediment. Petrol.* **1986**, *3*, 442–454. [[CrossRef](#)]
- Klemme, H.D.; Ulmishek, G.F. Effective Petroleum Source Rocks of the World: Stratigraphic Distribution and Controlling Depositional Factors. *AAPG Bull.* **1991**, *12*, 1809–1851.
- Warren, J.K. *Evaporites: Sediments, Resources and Hydrocarbons*; Springer Science & Business Media: Berlin, Germany, 2006.
- Friedman, G.M.; Handford, C.R.; Loucks, R.G.; Davies, G.R. Evaporites as Source Rock for Petroleum. In *Depositional and Diagenetic Spectra of Evaporites—A Core Workshop*; SEPM Society for Sedimentary Geology: Tulsa, Oklahoma, 1982.
- Grishina, S. Organic inclusions in salt. Part 3. Oil and gas inclusions in Cambrian evaporite deposit from East Siberia. A contribution to the understanding of nitrogen generation in evaporites. *Org. Geochem.* **1998**, *28*, 297–310. [[CrossRef](#)]
- Harris, N.B.; Freeman, K.H.; Pancost, R.D.; White, T.S.; Mitchell, G.D. The character and origin of lacustrine source rocks in the Lower Cretaceous synrift section, Congo Basin, west Africa. *AAPG Bull.* **2004**, *88*, 1163–1184. [[CrossRef](#)]
- Jin, Q.; Zhu, G.Y. Progress in Research of Deposition of Oil Source Rocks in Saline Lakes and Their Hydrocarbon Generation. *Geol. J. China Univ.* **2006**, *12*, 483–492, (In Chinese with English abstract).
- Hussain, M.; Warren, J.K. Source rock potential of shallow-water evaporites: An investigation in Holocene-Pleistocene salt flat sabkha (Playa), west Texas-New Mexico. *Carbonates Evaporites* **1991**, *2*, 217–223. [[CrossRef](#)]
- Katz, B.J. Lacustrine basin hydrocarbon exploration—current thoughts. *J. Paleolimnol.* **2001**, *26*, 161–179. [[CrossRef](#)]
- Huc, A.Y. Petroleum in the South Atlantic. *Oil Gas Sci. Technol.* **2004**, *59*, 243–253. [[CrossRef](#)]
- Li, Y.; Zhong, J.H.; Wen, Z.F.; Duan, H.L.; Wang, H.Q. Study on the Relationship between Evaporate and Hydrocarbon Generation. *Acta Sedimentol. Sin.* **2006**, *24*, 596–606.
- Hardie, L.A.; Eugster, H.P. The depositional environment of marine evaporites: A case for shallow, clastic accumulation. *Sedimentology* **2010**, *16*, 187–220. [[CrossRef](#)]

17. Figueiredo, F.T.; Almeida, R.P.; Freitas, B.T.; Marconato, A.; Carrera, S.C.; Turra, B.B. Tectonic activation, source area stratigraphy and provenance changes in a rift basin: The Early Cretaceous Tucano Basin (NE-Brazil). *Basin Res.* **2016**, *28*, 433–445. [[CrossRef](#)]
18. Zhu, D.Y.; Meng, Q.Q.; Jin, Z.J.; Liu, Q.Y.; Hu, W.X. Formation mechanism of deep Cambrian dolomite reservoirs in the Tarim basin, northwestern China. *Mar. Pet. Geol.* **2015**, *59*, 232–244. [[CrossRef](#)]
19. Shen, A.J.; Zheng, J.F.; Chen, Y.; Ni, X.; Huang, L. Characteristics, origin and distribution of dolomite reservoirs in Middle-Lower Cambrian, Tarim Basin, NW China. *Pet. Explor. Dev.* **2016**, *43*, 375–385. [[CrossRef](#)]
20. Du, J.H.; Pan, W.Q. Accumulation conditions and play targets of oil and gas in the Cambrian subsalt dolomite, Tarim Basin, NW China. *Pet. Explor. Dev.* **2016**, *43*, 360–374. [[CrossRef](#)]
21. Zhu, G.Y.; Chen, F.R.; Wang, M.; Zhang, Z.Y.; Ren, R.; Wu, L. Discovery of the lower Cambrian high-quality source rocks and deep oil and gas exploration potential in the Tarim Basin, China. *AAPG Bull.* **2018**, *102*, 2123–2151. [[CrossRef](#)]
22. Zhang, J.Z.; Wang, Z.M.; Yang, H.J.; Xu, Z.M.; Xiao, Z.Y.; Li, Z.X. Origin and differential accumulation of hydrocarbons in Cambrian sub-salt dolomite reservoirs in Zhongshen Area, Tarim Basin, NW China. *Pet. Explor. Dev.* **2017**, *44*, 40–47. [[CrossRef](#)]
23. Li, W.Q.; Guo, W.; Sun, S.L.; Yang, X.H.; Liu, S.; Hou, X.Y. Research on Hydrocarbon Accumulation Periods of Palaeozoic Reservoirs in Bachu-Maigaiti Area of Tarim Basin. *J. Jilin Univ.* **2018**, *48*, 640–651.
24. Deng, Q.; Zhang, H.Z.; Wang, H.Z.; Wei, Z.W.; Cheng, B.; Li, S.D.; Wang, Y.P.; Faboya, O.L.; Liao, Z.W. Organic Matter Accumulation Mechanism in the Lower Cambrian Strata from Well Luntan 1 in the Tarim Basin, NW China. *Geofluids* **2021**, *2021*, 1–13.
25. Guo, C.; Chen, D.Z.; Qing, H.R.; Dong, S.F.; Li, G.R.; Wang, D.; Qian, Y.X.; Liu, C.G. Multiple dolomitization and later hydrothermal alteration on the Upper Cambrian-Lower Ordovician carbonates in the northern Tarim Basin, China. *Mar. Pet. Geol.* **2016**, *72*, 295–316. [[CrossRef](#)]
26. Zhu, W.B.; Zheng, B.H.; Shu, L.S.; Ma, D.S.; Wu, H.L.; Li, Y.X.; Huang, W.T.; Yu, J.J. Neoproterozoic tectonic evolution of the Precambrian Aksu blueschist terrane, northwestern Tarim, China: Insights from LA-ICP-MS zircon U–Pb ages and geochemical data. *Precambrian Res.* **2011**, *185*, 215–230. [[CrossRef](#)]
27. Lu, Y.Z.; Zhu, W.B.; Ge, R.F.; Zheng, B.H.; He, J.W.; Diao, Z.P. Neoproterozoic active continental margin in the northwestern Tarim Craton: Clues from Neoproterozoic (meta)sedimentary rocks in the Wushi area, northwest China. *Precambrian Res.* **2017**, *298*, 88–106. [[CrossRef](#)]
28. Lin, C.S.; Yang, H.J.; Liu, J.Y.; Peng, L.; Cai, Z.Z.; Yang, X.F.; Yang, Y.H. Paleostuctural geomorphology of the Paleozoic central uplift belt and its constraint on the development of depositional facies in the Tarim Basin. *Sci. China Ser. D Earth Sci.* **2009**, *52*, 823–834. [[CrossRef](#)]
29. Zhao, G.C.; Wang, Y.J.; Huang, B.C.; Dong, Y.P.; Li, S.Z.; Zhang, G.W.; Yu, S. Geological reconstructions of the East Asian blocks: From the breakup of Rodinia to the assembly of Pangea. *Earth Sci. Rev.* **2018**, *186*, 262–286. [[CrossRef](#)]
30. Yang, Y.J. The Research on Lithofacies Paleogeography of Sequence and Characteristics of Source-Reservoir-Cap Assemblage of Cambrian in Tarim Basin. Ph.D. Thesis, Chengdu University of Technology, Chengdu, China, 2011.
31. Lin, C.S.; Li, S.T.; Liu, J.Y.; Qian, Y.X.; Luo, H.; Chen, J.Q.; Peng, L.; Rui, Z.F. Tectonic framework and paleogeographic evolution of the Tarim basin during the Paleozoic major evolutionary stages. *Acta Petrol. Sin.* **2011**, *27*, 210–218.
32. Zhou, X.Q.; Chen, D.Z.; Qing, H.R.; Qian, Y.X.; Wang, D. Submarine silica-rich hydrothermal activity during the earliest Cambrian in the Tarim Basin, Northwest China. *Int. Geol. Rev.* **2014**, *56*, 1906–1918. [[CrossRef](#)]
33. Jiang, L.; Worden, R.H.; Cai, C.F.; Shen, A.; Crowley, S.F. Diagenesis of an evaporite-related carbonate reservoir in deeply buried Cambrian strata, Tarim Basin, northwest China. *AAPG Bull.* **2018**, *102*, 77–102. [[CrossRef](#)]
34. Zheng, J.F.; Yuan, W.F.; Huang, L.L.; Pan, W.Q.; Qiao, Z.F.; Yang, G. Sedimentary facies model and its exploration significance of the Lower Cambrian Xiaerblak Formation in Xiaerblak area, Tarim Basin. *J. Palaeogeogr.* **2019**, *21*, 589–602.
35. Zhang, Y. Research on Dolomite Diagenesis of Cambrian Formation in Central Uplift Belt, Tarim Basin. Master Thesis, Xi'an Shiyou University, Xi'an, China, 2019.
36. You, X.L.; Sun, S.; Lin, C.S.; Zhu, J.Q. Microbial dolomite in the sabkha environment of the middle Cambrian in the Tarim Basin, NW China. *Aust. J. Earth Sci.* **2018**, *65*, 109–120. [[CrossRef](#)]
37. Zhang, S.C.; Liang, D.G.; Zhang, D.J. Evaluation criteria for Paleozoic effective hydrocarbon source rocks. *Pet. Explor. Dev.* **2002**, *29*, 8–12, (In Chinese with English abstract).
38. Zhaoyun, W.; Wenzhi, Z.; Yunpeng, W. Evaluation criteria for gas source rocks of marine carbonate in China. *Prog. Nat. Sci.* **2005**, *15*, 810–817. [[CrossRef](#)]
39. Guo, T.L. Geological Characteristics and Exploration Prospect of Carbonate Source Rock Gas in Sichuan Basin. *J. Southwest Pet. Univ.* **2021**, *43*, 1–16, (In Chinese with English abstract).
40. Stanley, R.G.; Valin, Z.C.; Pawlewicz, M.J. *Rock-Eval Pyrolysis and Vitrinite Reflectance Results from Outcrop Samples of the Rincon Shale (Lower Miocene) Collected at the Tajiguas Landfill, Santa Barbara County, California*; US Department of the Interior, US Geological Survey: Washington, DC, USA, 1992.
41. Hu, T.; Pang, X.Q.; Jiang, S.; Wang, Q.F.; Xu, T.W.; Lu, K.; Huang, C.; Chen, Y.Y.; Zheng, X.W. Impact of Paleosalinity, Dilution, Redox, and Paleoproductivity on Organic Matter Enrichment in a Saline Lacustrine Rift Basin: A Case Study of Paleogene Organic-Rich Shale in Dongpu Depression, Bohai Bay Basin, Eastern China. *Energy Fuels* **2018**, *32*, 5045–5061. [[CrossRef](#)]

42. Hu, S.Y.; Shi, S.Y.; Wang, T.S.; Liu, W.; Bai, B.; Xu, A.N.; Tu, J.Q.; Huang, S.P.; Jiang, H. Effect of gypsum-salt environment on hydrocarbon generation, reservoir-forming and hydrocarbon accumulation in carbonate strata. *China Pet. Explor.* **2016**, *21*, 20–27, (In Chinese with English abstract).
43. Warren, J.K. *Evaporites: A Geological Compendium*; Springer: Cham, Switzerland, 2016.
44. Wang, F.; Liu, X.C.; Deng, X.Q.; Li, Y.H.; Tian, J.C.; Li, S.X.; You, J.Q. Geochemical Characteristics and Environmental Implications of Trace Elements of Zhifang Formation in Ordos Basin. *Acta Sedimentol. Sin.* **2017**, *35*, 1265–1273, (In Chinese with English abstract).
45. Wei, K.; Li, X.B.; Liu, A.; Li, J.T.; Bai, Y.S.; Zhou, P.; Chen, X.H. Trace element characteristics of carbonate rocks from the Ediacaran Doushantuo Formation of Xikou section, Cili County, Hunan Province and its palaeoenvironmental significance. *J. Palaeogeogr.* **2015**, *17*, 297–308, (In Chinese with English abstract).
46. Lewan, M.D.; Maynard, J.B. Factors controlling enrichment of vanadium and nickel in the bitumen of organic sedimentary rocks. *Geochim. Cosmochim. Acta* **1982**, *46*, 2547–2560. [[CrossRef](#)]
47. Ding, J.; Zhang, J.; Tang, X.; Huo, Z.; Han, S.; Yue, L.; Zheng, Y.; Xingqi, L.; Liu, T. Elemental Geochemical Evidence for Depositional Conditions and Organic Matter Enrichment of Black Rock Series Strata in an Inter-Platform Basin: The Lower Carboniferous Datang Formation, Southern Guizhou, Southwest China. *Minerals* **2018**, *8*, 509. [[CrossRef](#)]
48. Wang, L.L.; Fu, Y.; Fang, S.J. Elemental geochemical characteristics and geological significance of Majiagou Formation, eastern Ordos Basin. *Pet. Geol. Exp.* **2018**, *40*, 519–525, (In Chinese with English abstract).
49. Zhang, W.H.; Tang, D.J.; Yang, Y.; Zhang, J.D.; Liu, X.F.; Wang, D.D.; Zeng, Q.N.; Liu, W.B. Sedimentary characteristics and hydrocarbon potential of Meso-Neoproterozoic source rocks in North China Platform. *Geol. China* **2020**, *36*, 1–18, (In Chinese with English abstract).
50. Zhu, L.X.; Tan, F.W.; Chen, M.; Fu, X.G.; Feng, X.L. Trace element in carbonate rocks and the palaeoenvironment during the Late Jurassic-Early Cretaceous in the Nadigangri area of Qiangtang Basin, China. *J. Chengdu Univ. Technol.* **2011**, *38*, 549–556, (In Chinese with English abstract).
51. Deng, X.; Kang, Z.H.; Peng, Y.Y.; Xiao, H.F.; Han, H.Y.; Yu, X.D. Shales of Wufeng Formation in Southern Sichuan Basin Indicate Paleoproductivity and Palaeohydrological Depth of Field. *Coal Technol.* **2018**, *37*, 122–124, (In Chinese with English abstract).